View metadata, citation and similar papers at core.ac.uk
brought to you by CORE
provided by CERN Document Server

Beam loss monitors

K. Wittenburg
DESY, Hamburg, Germany

Abstract
This lecture covers the fundamental aspects of the measurement of beam losses including their use for beam diagnostic and safety issues. The detailed functionality and detection principle of various common beam loss monitors are also presented, with a focus on their intrinsic sensitivity.

1 Introduction

Beam loss monitor systems are typically designed for measuring the amount and location of beam losses along an accelerator or storage ring. An appropriate design of such a system depends on various aspects, in particular:

– What kind of beam losses are to be detected?

– A detailed understanding of the beam loss mechanism and the adjacent processes which make a beam loss detectable by the loss monitors and

– The type of beam loss monitor.

This lecture discusses these three important aspects. Since each topic could be a lecture on its own, this paper is supported by many references which go into more depth on these topics. Many of these references can be found online on the JACoW site (http://acccelconf.web.cern.ch/AccelConf/).

This lecture is divided into three parts, with its main focus on point 3.

1. Loss classes: different kinds of beam loss are discussed to give a feeling for the wide range of applications of beam loss monitors and to motivate the following two topics.
2. Principles of loss detection: the fundamental aspects of measuring beam losses are discussed.
3. Beam loss monitors (BLMs): some typical BLMs are discussed with the focus on their sensitivity.

2 Loss classes

In the first section I would like to discuss some examples of interesting measurements and applications for BLMs.

Beam losses are divided into two different classes, namely irregular losses and regular losses [1]. The specification for *acceptable* beam losses as a function of beam momentum (see Section 2.1) and the *minimum required sensitivity* defines the dynamic range for the BLMs. Additional sensitivity combined with a larger dynamic range extends the utility of BLM systems for diagnostic work (Section 2.2).

2.1 Irregular beam losses

This class of losses (sometimes also called uncontrolled or fast losses) contains avoidable (!) losses of higher levels which are often the result of a misaligned beam or of a faulty condition of accelerator elements. A typical example is a trip of the RF which, in electron storage rings, causes fast beam loss

as a result of the energy loss of the electrons; vacuum problems also fall into this category. These losses may be distributed around the machine. A well designed collimator system might capture most of the losses, but even then a fraction of the losses may cause problems at other locations. Very often the BLMs are part of the machine protection system [2] to keep those losses below a certain level in order to avoid beam-loss-related 'damage' of components. However, irregular losses sometimes have to be tolerated even at high levels during machine studies or commissioning. In any case a BLM system has to define the allowed level of such losses in order to protect the machine against serious damage. A post mortem event analysis is most helpful to understand and analyse the faulty conditions.

2.1.1 Some examples of irregular beam losses

2.1.1.1 Superconducting machines: quench protection

Superconducting accelerators need a dedicated BLM system to prevent beam-loss-induced quenches. Such a system has to detect losses fast enough before they lead to a high energy deposition in the superconducting material which might lead to a quench. Examples of such systems can be found at the HERA, the Tevatron and the LHC [2–4]. Typically, a BLM system implements several individual thresholds for the amount of beam losses, and automatically dumps the beam if one or more of them are exceeded. The thresholds can depend on various conditions, e.g., the beam energy, the BLM position, the allowed heat deposition in the superconductor. Figure 1 shows an example of a post mortem archive of a beam loss in the HERA superconducting proton ring. To prevent unwanted beam dumps due to faulty conditions of one BLM, it might be useful to add another threshold for how many BLMs have to be above their individual threshold before a dump is triggered. In this case one might have to multiply the amount of BLMs at critical locations by that number to ensure safe conditions even with very localized beam losses or at very sensitive locations (e.g., high lattice dispersion in superconducting magnets).

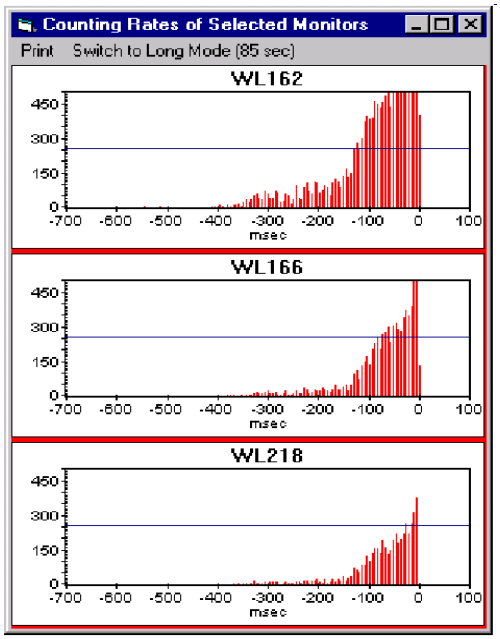

Fig. 1: Beam losses in HERAp. Each vertical line corresponds to a beam loss rate within 5.2 ms. The horizontal line indicates the individual threshold of each BLM (three BLMs at different locations are shown). After four BLMs reached their individual threshold (horizontal line) the beam was dumped by the system in order to protect the magnets from quenching. The history of the last 700 ms before the dump and 100 ms after the dump are shown.

2.1.1.2 Activation of environment due to losses

The activation of components should be kept low enough for hands-on maintenance [typically no more than 0.1 rad/h residual activation (30 cm from surface, after 4 h cool-down)], personal safety, and environmental protection. As a rule of thumb this value means for a hadron accelerator an allowed slow beam loss rate of about 1 W/m or for a 1 GeV hadron accelerator a loss rate of about 13 particles/m at 500 MHz. For electron accelerators the rates might be higher. Figure 2 shows as an example the strong correlation between measured losses and residual activation at KEK. To avoid activation the loss rate should be kept as low as possible with the help of a BLM system.

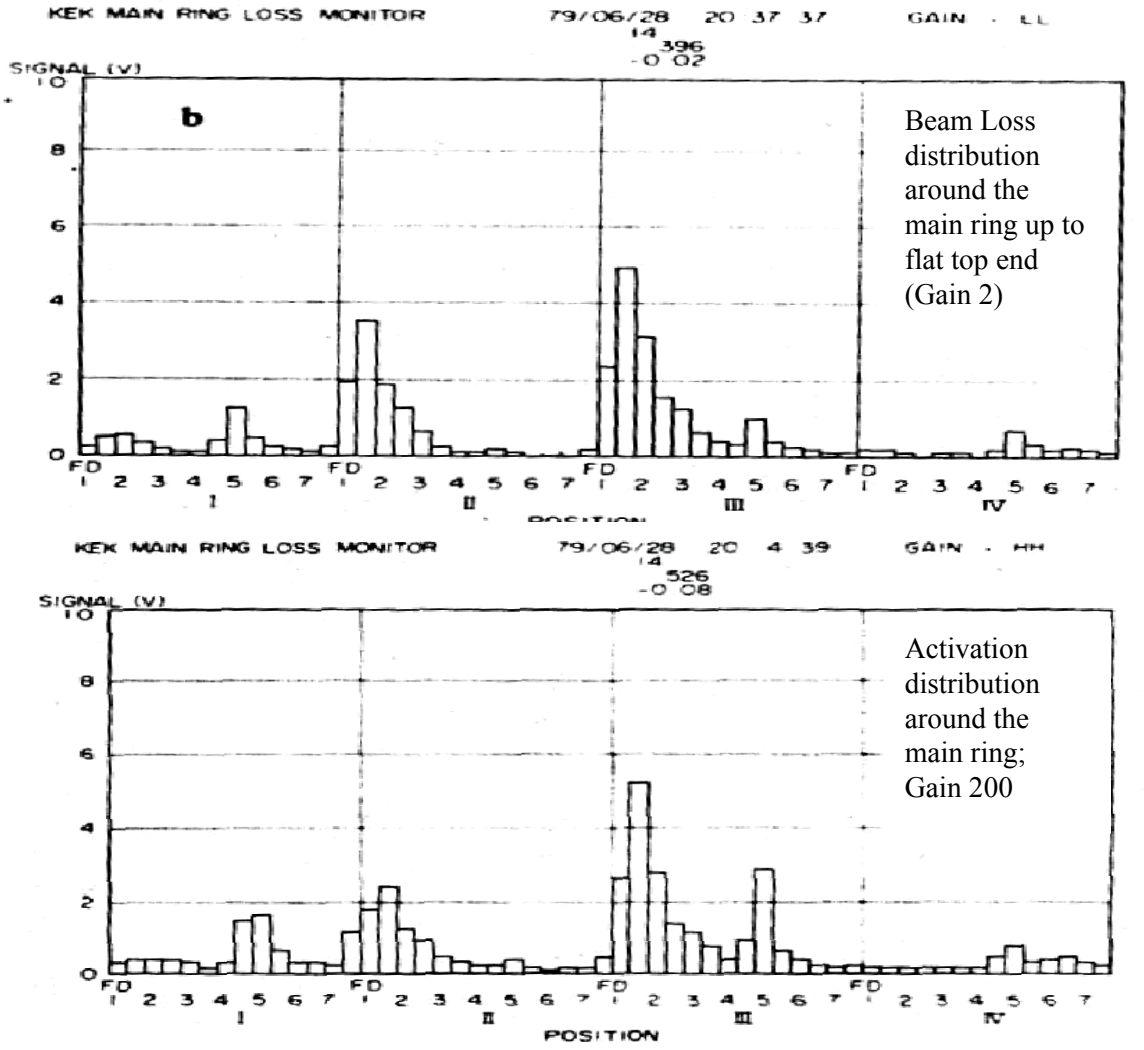

Fig. 2: Correlation between beam losses (upper part) and activation (lower part) at KEK measured by beam loss monitors [5]

2.1.1.3 Commissioning: obstacles

During commissioning of an accelerator a BLM system can be most helpful in detecting several problems which might prevent circulating beam. Typical examples are badly connected RF fingers which point into the beam pipe and act as a target for the beam (not to mention the empty beer bottle in the LEP beam pipe). The readings of the BLMs around the ring showed such an obstacle during the commissioning of the RHIC ring [6], see Fig. 3. This made the localization of the problem much easier, even a steering of the beam with a local bump around this obstacle immediately provided circulating beam.

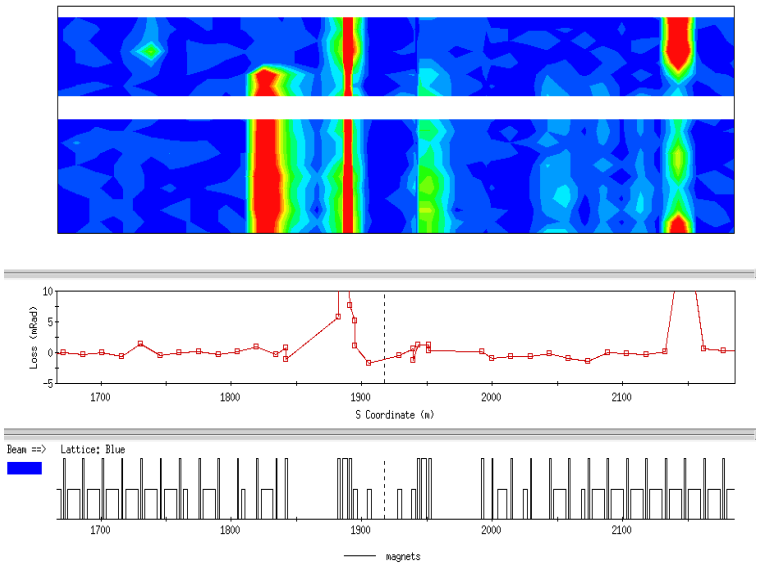

Fig. 3: Loss pattern evolution in RHIC as beam was steered locally around an apparent obstacle at $s \simeq 1820$ m. When the losses there went away, beam began circulating for thousands of turns. From Ref. [6].

2.1.1.4 Vacuum problems (Coulomb scattering)

BLMs can help to detect even very small vacuum leaks. Beam particles scatter on the residual gas, so a pressure bump can be seen from a higher loss rate in that area. Figure 4 shows an example from HERAe, where the ring-wide BLM system detected a higher loss rate at two locations, which were correlated with two small vacuum leaks. After the repair, the life time τ of the beam immediately increased to the original value.

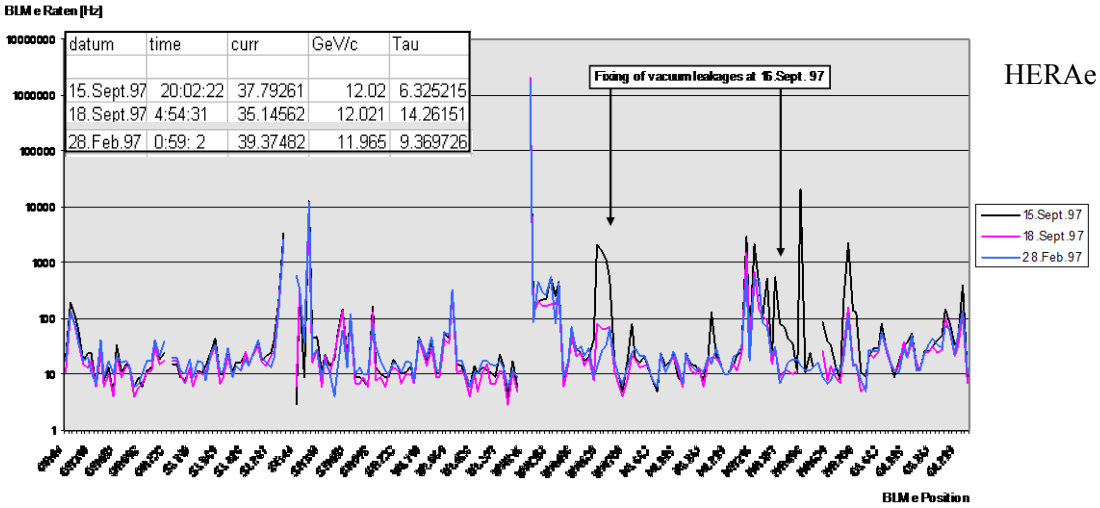

Fig. 4: Two vacuum leaks detected by the BLM measurements at HERAe in September 1997. The BLM rates are plotted on the vertical scale, on the horizontal axis are the BLM locations around the whole circumference of the ring. The leak was detected on 15 September 1997 and fixed on 16 September 1997. On 18 September 1997 the loss rates were back to the original rates measured on 28 February 1997.

2.1.1.5 Microparticles

Unexpected reversible and irreversible jumps in the lifetime were observed when operating HERAe with electrons [7] (Fig. 5). The BLMs were most helpful for a better understanding of this problem. They localized very precisely the origin of the jumps, which turned out to be microparticles emitted from ion getter pumps. By switching off the dominant pumps the effect could be reduced.

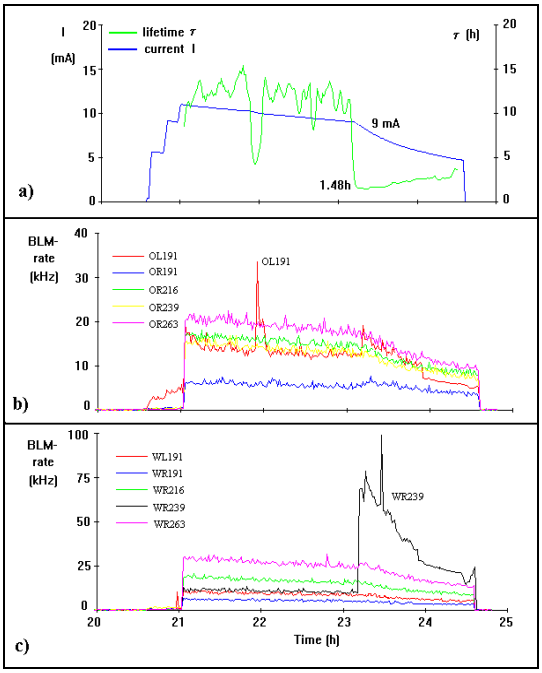

Fig. 5: From Ref. [7]. Lifetime reduction events correlate well with losses seen in the HERA electron loss monitors. In this example a brief disruption of lifetime is seen in the loss monitor OL191, and an irreversible disruption is seen in the monitor WR239.

2.1.1.6 High current and high brilliance machines (ring or linac): destruction of vacuum components

A serious problem for high current and high brilliance accelerators is the high power density of the beam. A misaligned beam is able to destroy the beam pipe or collimators and may break the vacuum (Fig. 6). This fact makes the BLM system one of the primary diagnostic tools for beam tuning and equipment protection in these machines.

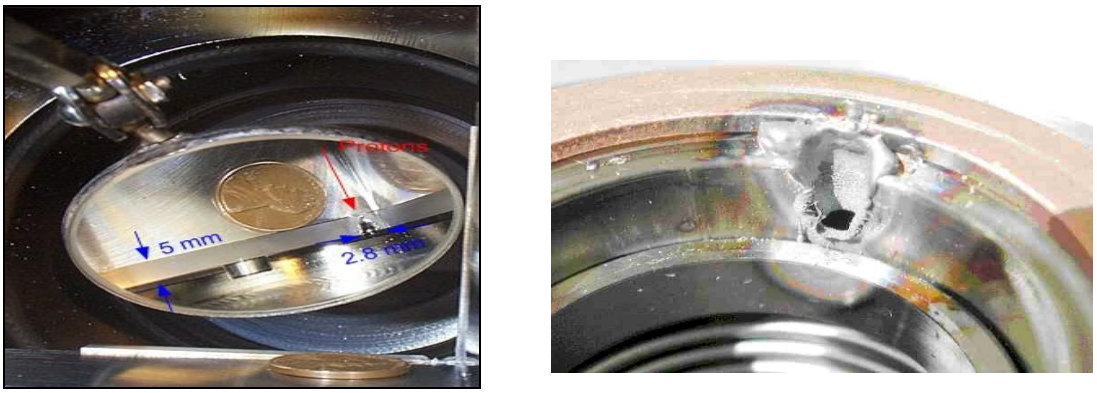

Fig. 6: Both figures show serious damage to vacuum components in the Tevatron [8] (left) and ELBE [9] (right) due to direct beam impact. In both cases no BLM system was available at the time.

2.2 Regular beam losses

Regular losses (sometimes also called controlled or slow losses) are typically not avoidable and are localized on the collimator system or on other (hopefully known) aperture limits. They might occur continuously during operation and correspond to the lifetime/transport efficiency of the beam in the accelerator. The lowest possible loss rate is defined by the theoretical beam lifetime limitation due to various effects, e.g., Touschek effect, beam–beam interactions, collisions, transversal and longitudinal diffusion, residual gas scattering, halo scraping, instabilities. These losses are suitable for machine diagnostics with a BLM system.

2.2.1 Some examples of regular beam losses

2.2.1.1 Injection studies

BLMs are useful to improve the injection efficiency, even at low injection current (radiation safety issue). They are more sensitive than current transformers and they can distinguish between transversal mismatch (high losses at high beta values) and energy mismatch (high losses at high dispersion values) and unpredicted small apertures (losses somewhere else).

Figure 7 shows an example from the ALS [10]. Several BPMs report high count rates at injection. From this graph one can identify the sites of the highest beam loss. Several peaks result from different centres of beam loss. An online optimization of the injection elements is possible by minimizing these loss rates.

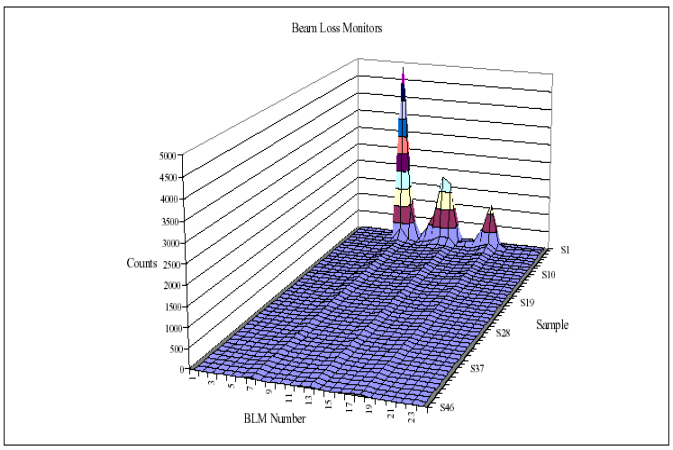

Fig. 7: Surface plot of beam loss at injection [10]

2.2.1.2 Lifetime limitations (Touschek effect, etc.)

In addition to faulty conditions, there are unavoidable effects which limit the beam lifetime in an accelerator, e.g., vacuum lifetime (Coulomb scattering), Touschek effect, quantum lifetime.

Good BLM locations for the detection of Touschek scattered particles are high dispersion sections which follow sections where a high particle density was reached. Since the two colliding particles lose and gain an equal amount of momentum, they will hit the inside and outside walls of the vacuum chamber. In contrast, elastically or inelastically scattered particles [residual gas atoms (Coulomb) or photons (Compton) or high-energy synchrotron radiation photons (Quantum)] are lost at aperture limits. If the energy carried away from the beam particle is too large, the particle gets lost after the following bending magnet only on the inside wall of the vacuum chamber. A BLM system with good selectivity to the different loss mechanisms is a very useful tool for various kinds of beam diagnostics, especially in Touschek limited (electron-) accelerators: the Touschek loss rate depends on the 3-dimensional electron density and on the spin of the scattering particles. Therefore any change in

one or more of these parameters has an influence on the loss rates at the selected monitors. An example is shown in Fig. 8 where the BLM system at BESSY was used to determine the (desired) vertical beam blow-up due to a resonant head–tail mode excitation [11]. BLM systems were also used to calibrate precisely the beam energy and observe its variation in time by using resonant depolarization of the beam [11, 12].

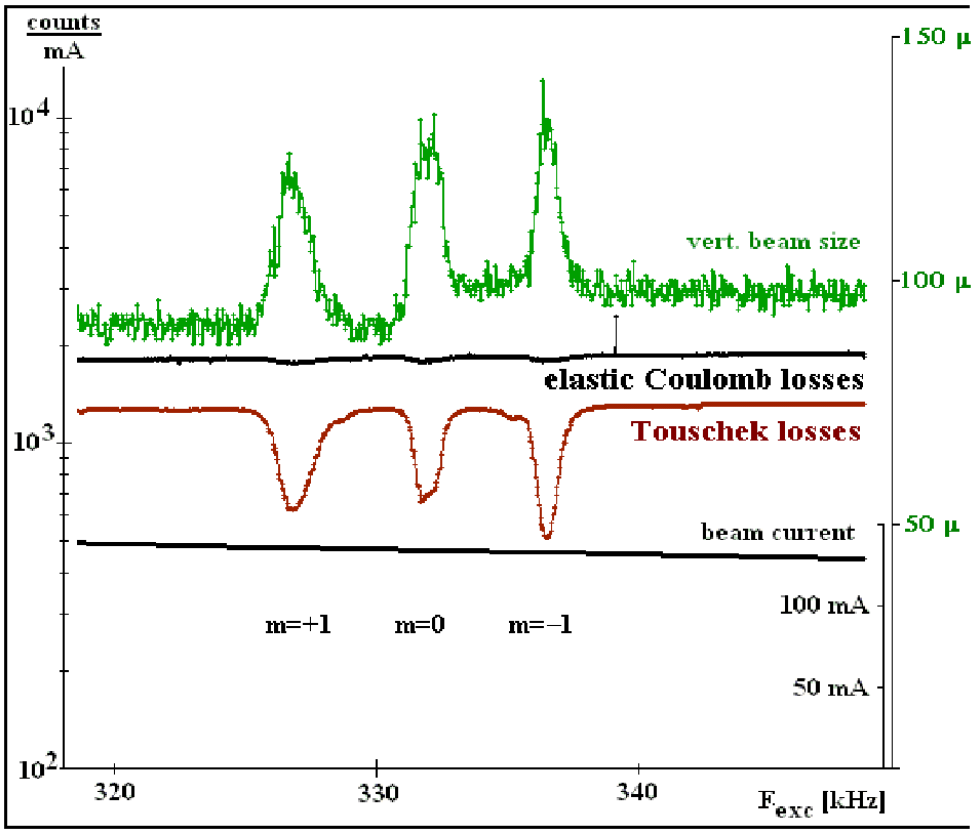

Fig. 8: Vertical beam size, Touschek and Coulomb loss rates during excitation of a vertical head–tail mode in BESSY [11]. Clearly observable is the decrease of the Touschek loss rate (BLMs at the outside of the ring) with increasing vertical beam size, while the Coulomb losses stay nearly constant (BLMs on the inside of the ring).

2.2.1.3 Tail measurements

Non-Gaussian tails in the beam distribution produce lower beam lifetimes and background in experimental detectors. These tails are difficult to detect with standard beam profile monitors because of their small population with respect to the core of the beam [13]. A combination of scrapers and BLMs is a very sensitive way to measure tail populations. The measurement and scraping can be done by moving the scraper closer to the beam core in small steps, measuring at each step the response of the adjacent BLM. The movement of the scraper can be adjusted according to the loss rate to avoid scraping the beam core. Reference [14] shows measurements at LEP where the dominant processes of tail creation were Compton scattering on thermal photons (horizontal) and beam–beam bremsstrahlung (vertical).

In high-energy proton accelerators, lifetime limitations may arises from proton diffusion due to beam–beam interactions and tune modulation due to ground motion. The ground motion frequencies and diffusion parameters can be measured with BLMs at the collimators [15, 16]. Figure 9 shows BLM measurements at HERAp where the frequency spectrum of the measured losses of a very stable beam corresponds very well to that of the ground motion.

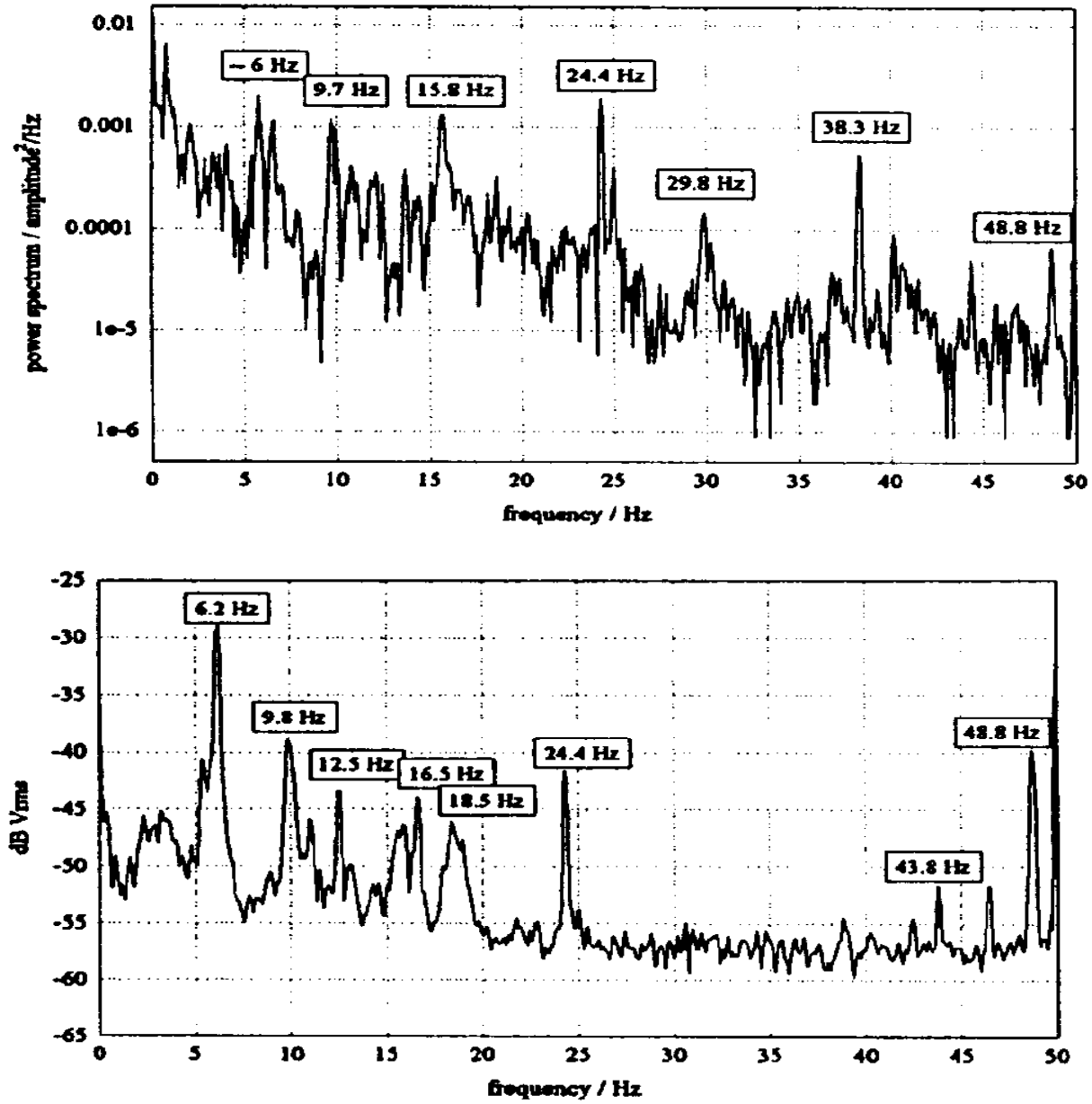

Fig. 9: Frequency spectrum of ground motion (upper) and frequency spectrum of losses at a collimator (lower), from Ref. [16].

2.2.1.4 Tune scans

Regular losses can also be used for optimizing the machine lattice by studying the tune dependence of the losses [17]. A tune scan is also useful for studying nonlinear resonances caused by insertion devices [18]. Figure 10 shows the scanning of the various tunes in both planes and their corresponding beam loss rates. In this example a $Q_x + 3Q_y$ resonance was clearly identified which causes harmful beam losses at a certain location (equipped with a BLM) in BESSY. The localization of a certain loss is clearly an advantage with respect to a beam lifetime measurement which does not provide position information. With the help of BLMs tune scans can be made faster because the sensitive direct loss measurement is faster than a precise lifetime determination.

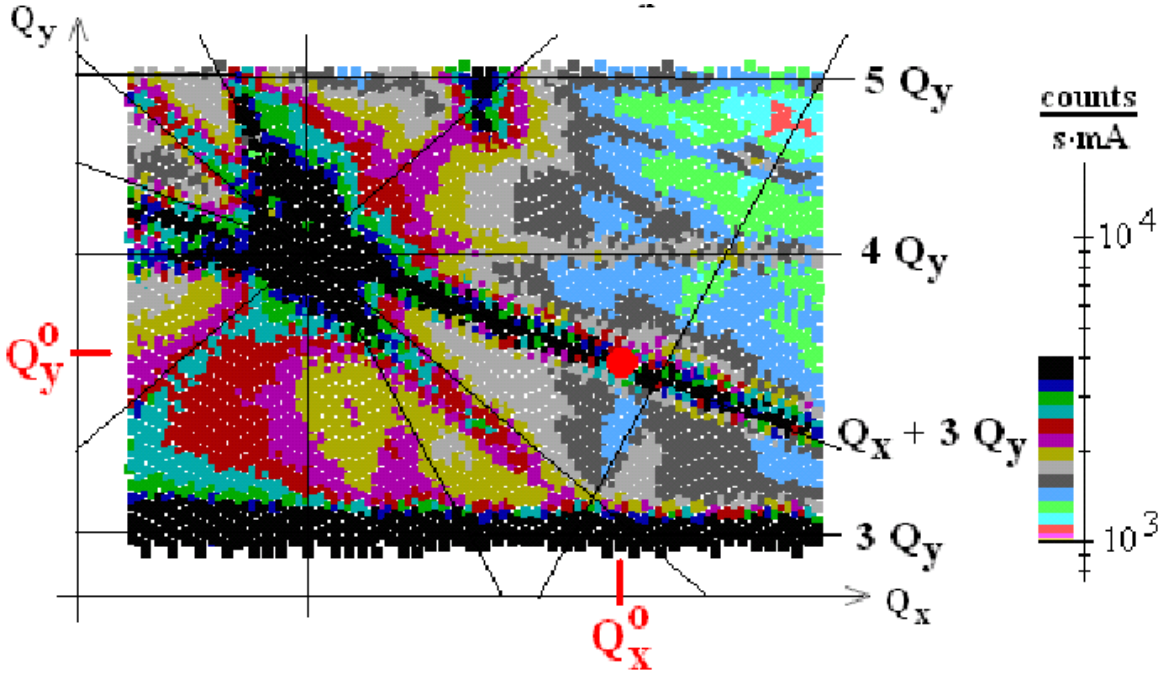

Fig. 10: Two-dimensional tune scan at BESSY [17]

3 Principles of loss detection

This section describes some common aspects of beam loss measurements. Note that systems like differential beam current measurements and dose measurements (or activation) are not the subject of this session. They have a very rough position resolution or a very long time constant, respectively. This session concentrates on dedicated beam loss measurements with some numbers of BLMs and a time resolution in the order of some turns or even faster, up to bunch-by-bunch resolution. BLMs at special locations may serve also for dedicated beam studies as explained in the previous section.

3.1 Considerations in selecting a beam loss monitor

R.E. Shafer gave a very good tutorial about beam loss monitoring at the 2002 Beam Instrumentation Workshop [19] where he summarized the important factors for selecting the right type of BLM for a specific application. Consideration of these parameters gives a good guide to finding (or designing) the best monitor type for a particular beam loss application:

- *Intrinsic sensitivity*
- Type of output (current or pulse)
- Ease of calibration (online)
- System end-to-end online tests
- Uniformity of calibration (unit to unit)
- Calibration drifts due to ageing, radiation damage, out-gassing, etc.
- *Radiation hardness (material)*
- Reliability, availability, maintainability, inspectability, robustness
- Cost (incl. electronics)
- Shieldability from unwanted radiation (synchrotron radiation)
- *Physical size*
- Spatial uniformity of coverage (e.g., in long tunnel, directionality)
- Dynamic range (rads/s and rads)
- *Bandwidth* (temporal resolution)
- Response to low duty cycle (pulsed) radiation

- Instantaneous dynamic range (vs. switched gain dynamic range)
- Response to excessively high radiation levels (graceful degradation)
- Signal source
- Positioning

In the discussion of some BLM types in Section 4, I shall stress the topics in italics a little bit more while the last two topics are discussed in Sections 3.2 and 3.3.

3.2 The signal source or what should a beam loss monitor monitor?

In case of a beam loss, a BLM has to establish the number of lost particles in a certain position and time interval. A typical BLM is mounted outside of the vacuum chamber, so that the monitor normally observes the shower caused by the lost particles interacting in the vacuum chamber walls or in the material of the magnets. The number of detected particles (amount of radiation, dose) and the signal from the BLM should be proportional to the number of lost particles. This proportionality (or efficiency ε) in terms of signal/lost particle depends on the type of BLM (its intrinsic sensitivity S_{BLM}), the position of the BLM with respect to the beam, the type of the lost particles, and the intervening material. But also on the momentum of the lost particles, which may vary by a large ratio during the acceleration cycle. It is nearly impossible to *measure* the exact efficiency of BLMs around an accelerator because of the impossibility of generating beam losses at exactly one location in an accelerator since a significant amount of beam particles will be scattered and lost at other places at the same time. Therefore the usual way of defining the overall efficiency ε is to use Monte Carlo programs like EGS (for electrons), Fluka or Geant (for Hadrons) [20]. With the help of these programs one can simulate the particle loss at a certain location together with the whole geometry (beam pipe, magnets, valves) near the BLM, the corresponding magnet and electrical fields of accelerator components and the BLM itself (see Section 3.3). The amount of beam loss at a certain location is then defined as

$$\text{Number of lost particles } N = \mathit{Signal}/\varepsilon.$$

The signal of a BLM depends on the type of BLM and is typically a current or a count rate (see Section 3), in some cases it might be 'light' which is then converted to current by photosensitive elements like photomultipliers.

The common signal source of beam loss monitors is mainly the ionizing capability of the charged shower particles crossing the BLM. Their ionization loss is described by the Bethe–Bloch formula:

$$\boxed{\frac{\mathrm{d}E}{\mathrm{d}x} = \frac{4\pi}{m_e c^2} \cdot \frac{n Z^2}{\beta^2} \cdot \left(\frac{e^2}{4\pi\varepsilon_0}\right)^2 \cdot \left[\ln\left(\frac{2 m_e c^2 \beta^2}{I \cdot \left(1-\beta^2\right)}\right) - \beta^2\right]} \qquad (1)$$

With $\beta = v/c$ and $I \approx 16 \cdot Z^{0.9}$ eV. I is the mean excitation energy of the material of density p, atomic number Z, and atomic mass A.

There is a region at $\beta\gamma = p/m_0c \approx 2$ where $\mathrm{d}E/\mathrm{d}x$ reaches a minimum (see Fig. 11). A particle having a mean ionizing energy loss in the region of the minimum ionization is often called minimum ionizing particle or MIP. The value of the energy deposited by a MIP is $\mathrm{d}E/\mathrm{d}x_{\mathrm{MIP}} \approx$ 1–2 MeV/(g/cm^2) and is valid for many materials. Above this point there is a logarithmic increase of $\mathrm{d}E/\mathrm{d}x$ with energy, caused by relativistic effects. This increase is considered in the following to be negligible, so that MIP means a particle with $\beta\gamma = p/m_0c \geq 2$.

The energy from such an ionization loss can be used to create electron/ion pairs (current) or photons in the BLM detector material.

An energy deposition in (detector) material can be given in units of rad or Gy (= 100 rad). Using the definition of 1 rad = 100 ergs/gram and 1 MeV = $1.6 \cdot 10^{-6}$ ergs leads to another definition, in terms of MIPs/cm^2.

$$1\,\text{rad} = \frac{100\,\text{ergs}}{\text{gram}} \cdot \frac{1\,\text{MeV}}{1.6 \cdot 10^{-6}\,\text{ergs}} \cdot \frac{\text{MIP gram}}{2\,\text{MeV cm}^2} = 3.1 \cdot 10^7\,\frac{\text{MIP}}{\text{cm}^2} \tag{2}$$

(From Ref. [19])

The intrinsic sensitivity S_{BLM} of a beam loss monitor can now be described in terms of either energy deposition (rad) in a BLM, or in terms of a charged particle (MIPs) flux ($3.1 \cdot 10^7$ MIPs/cm^2) through a BLM (Section 4). But note that this relation is true only for a radiation field which contains MIPs only. This is nearly true for high-energy accelerators with the BLM close to the beam pipe. As pointed out before, a careful study by Monte Carlo simulations is recommended to get the real energy and particle spectrum of the radiation.

Another typical signal source of BLMs is the 'secondary emission' from (detector) surfaces. When a charged particle crosses a metallic surface, secondary electrons are emitted from it. The Sternglass formula describes the secondary emission coefficient of various materials in terms of 'number of emitted electrons' for primary electron, proton, and ion impacts [21, 22]. For many metals this coefficient is of the order of a few per cent per MIP (see Fig. 12).

Sometimes bremsstrahlung is used as a signal source, see, for example, Refs. [24, 25] but this method is not discussed here because of its very special application.

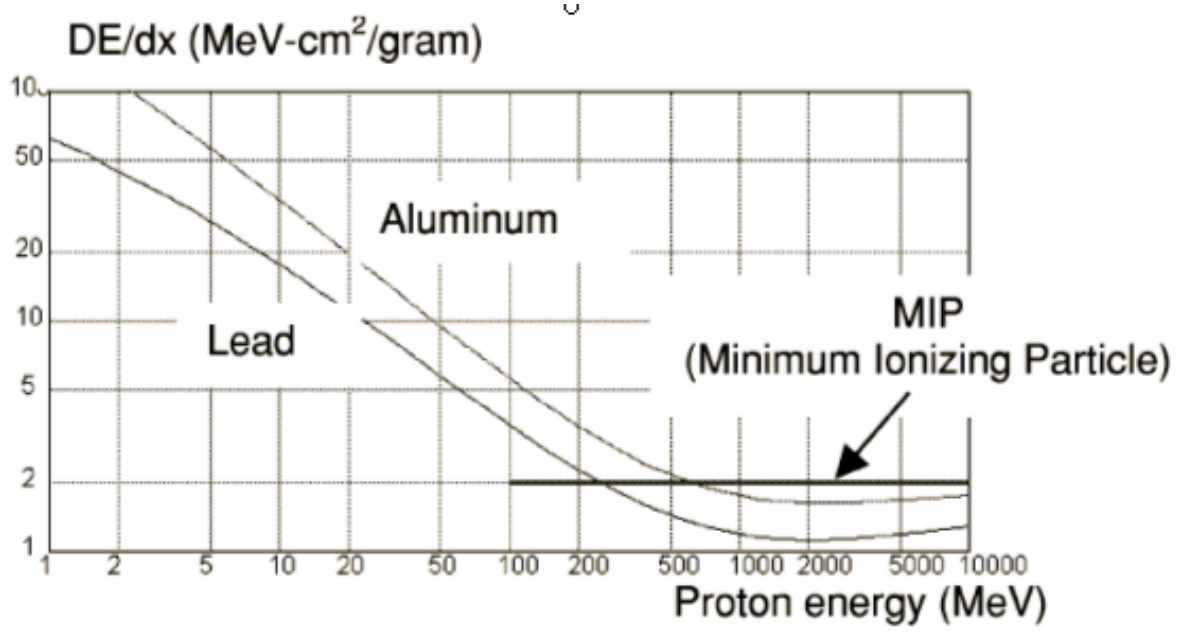

Fig. 11: The dE/dx [MeV/(g/cm^2)]for protons in lead vs. proton energy [MeV/c] (from Ref. [19]). Note that an electron with an energy of ≥ 1 MeV/c (≈ $2 \cdot p/m_0c$), for example, is also considered as a MIP with dE/dx ≈ 1–2 MeV/(g/cm^2) for many materials.

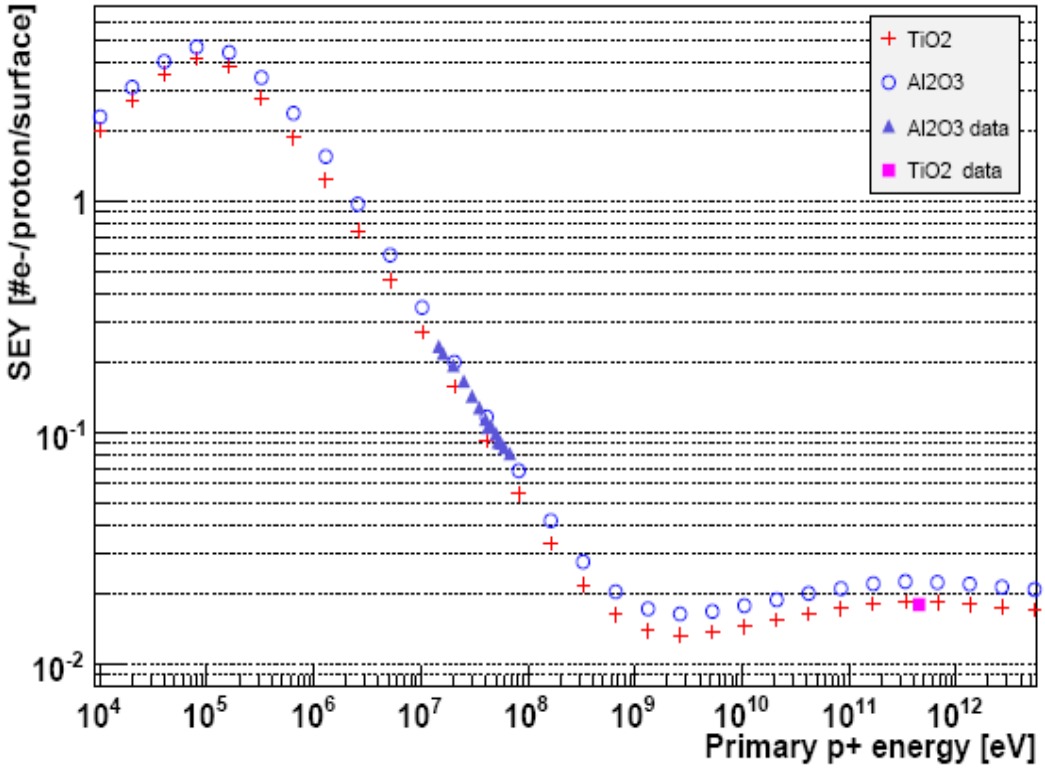

Fig. 12: Secondary emission coefficient vs. primary particle energy (here protons), from Ref. [23]

3.3 Positioning of beam loss monitors

Each BLM at each location needs its own specific efficiency calibration ε in terms of signal/lost particle. This calibration can be calculated using a Monte Carlo program using the (more or less) exact geometry and materials between the beam and the BLM. The loss of a high-energy particle in the wall of a beam pipe results in a shower of particles which leak out of the pipe (low-energy beam particles which do not create a shower leakage outside the vacuum pipe wall will hardly be detectable by a loss monitor system). The efficiency of a loss detector will be highest if it is located at the maximum of the shower. Examples can be found in Refs. [26–29] where Monte Carlo simulations were used to find the optimum locations for the monitors, as well as to calibrate the monitors in terms of 'lost particles/signal'. The length of the shower depends on the energy of the lost particle and ranges from some metres for very high proton energies [27, 28] to a few centimetres for medium electron energies [29]. Therefore the expected location of lost particles has to be studied in advance so as to situate the monitors at the right place, especially at electron accelerators. This implies that an understanding of the loss mechanism and dynamics in the accelerator are necessary to predict the typical positions of losses. For example, Refs. [28–30] report detailed particle tracking studies being done to follow the trajectory of an electron in the accelerator after an energy loss due to scattering on a residual gas molecule or on a microparticle. There are many different reasons for beam losses and a complete beam loss system has to be carefully designed for the detection and analysis of a specific loss mechanism (see examples in Section 2).

Figure 13 shows an example of beam losses due to inelastic scattering (on residual gas or microparticles). This example also shows that a distortion of the beam results in beam offsets which are largest in the middle of focusing quadrupoles. This is also true for the beam size, which is large at high β functions. Therefore the preferred locations for beam losses (and therefore for BLMs) might be aperture limits like collimators, scrapers, locations with high dispersion or high β functions. Since the quadrupoles always have a local β maximum, either in x or in y, they are the preferred locations for

BLMs around an accelerator. This is especially true for BLMs which have to serve the quench protection system in superconducting accelerators [2–4, 26]. Again, detailed Monte Carlo simulations can help find the optimum positions of BLMs at the superconducting quadrupoles as well as the efficiencies at these positions.

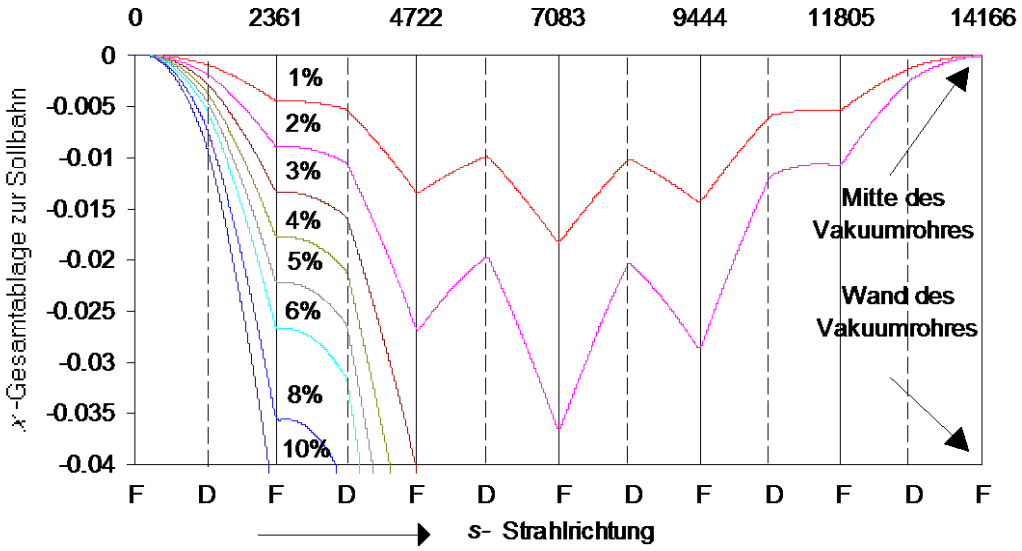

Fig. 13: The beam-electrons lose energy ΔE of between 1% and 10% due to inelastic scattering (bremsstrahlung) mainly on the nuclei of the residual gas molecules. The deviation of the electron orbit from the nominal orbit x along some FODO cells s depends on the dispersion function in the accelerator and on ΔE. Therefore the electrons may be lost at their aperture limit behind the following bending magnet on the inside wall of the vacuum chamber at 4 cm [30].

4 Types of beam loss monitors

In the following sections I discuss some typical BLM detectors with the emphasis on their intrinsic sensitivity S_{BLM}, but other aspects including radiation hardness, size, and temporal resolution are also treated. Additional overviews of BLMs and detectors can be found, for example, in Refs. [31, 32] and in various text books [33, 34].

4.1 Short ionization chamber

Short ionization chambers are used as BLMs in many accelerators. An ionization chamber in its simplest form consists of two parallel metallic electrodes (anode and cathode) separated by a gap of width D. The gap is filled with gas (air, argon, xenon[1]) or liquid of density ρ and defines the sensitive volume of the chamber. High voltages, V, up to several kV, are applied between the anode and cathode. Ionizing particles traversing the sensitive volume ionize the gas or liquid and produce electron–ion pairs. The electric field $E = V/D$ causes electrons and positive ions to drift in opposite directions toward the anode and cathode, respectively. The number of electrons reaching the anode depends on the applied voltage. If the voltage is very small, the electrons produced by ionization recombine with their parent ion. The electrons can escape this initial recombination if the electric field is larger than the Coulomb field in the vicinity of the parent ion. The number of electrons collected at the anode increases with voltage up to saturation where all charges are collected. In this *ionization*

[1] Avoid electronegative gases (O_2, H_2O, CO_2, SF_6 etc.), they capture electrons before reaching the electrode. Noble gases have negative electron affinities (Ar, He, Ne), better for the proportional region.

region the created charge should not depend on the applied voltage. At higher voltages, the electrons gain enough energy to produce ionization on their path which is called the *proportional region* and the *Geiger–Müller region* is where saturation is reached (see Fig. 14).

The flatness of the plateau of the ionization region depends on the collection efficiency of the electrons or ions on the electrodes. Especially at high radiation levels, electrons on their way to the anode may be captured by positive ions produced close to their trajectory (by other incoming particles) and do not contribute to the charge collection. Therefore high voltage and a small gap D are preferred to achieve a high dynamic range of an ionization chamber. This effect was well documented during the improvement of the ionization chamber BLM for SNS [35]. A smaller gap has an additional effect on the response time of a chamber: the response time is defined by the transit time t of the created charge through the gap (here for ions) [35]

$$t = D/v_{\text{ion}} = D^2/[\mu_0 V (P_0/P)]$$

with the ion speed:

$$v_{\text{ion}} = \mu_0 E(P_0/P) = \mu_0 (V/D)(P_0/P)$$

where μ_0 = ion mobility, V = voltage, P/P_0 = pressure (Atm), D = gap (for plane electrodes) or $D^2 = [(a^2 - b^2)/2] \ln (a/b)$ (for cylindrical geometry with a, b = radius of the inner and outer electrode).

The ion mobility μ_{ion} is for typical gases $\mu_{\text{ion}} = 1.0–1.5$ cm^2 atm/(V·s) which gives for $D = 1$ cm, $p = 1$ atm, $V = 1.5$ kV a response time of $t_\mu \approx$ 0.4–1 ms, which is often too slow for BLMs. The electron mobility μ_e is about 10^3 times faster than for ions, therefore

$$t_e \approx 0.4–1 \text{ μs}.$$

The signal of an ionization chamber is a combination of both and is shown in Fig. 15. Further improvement in speed was achieved for the LHC type of ionization chamber. Here pane electrodes have a smaller gap in a meander constellation to fill a volume of 1.5 L. A response time of 0.3 μs is achieved [37, 38]. A comparison between the SNS and LHC chambers is shown in Fig. 16.

Another important aspect is the dynamic range of the ionization chamber. The upper limit is given by the nonlinearity due to the recombination rate at high dose; the typical chamber current in such a case is a few hundred μA. The lower limit is given by the dark current between the two electrodes. A very careful design of the chamber is necessary for very low dark currents in the order of tens of pA or better. This gives a dynamic range of 10^6–10^8. Note that such a high dynamic range needs some special signal processing. Solutions like logarithmic amplifiers, high ADC resolution, current to frequency conversion and counting schemes [38] are reported.

Ionization chambers can be built from radiation-hard materials like ceramic, glass and metal with no radiation or time ageing. Special care has to be taken for the feedthroughs. Up to more than 10^8 rad can be tolerated by a careful design focused on radiation hardness. Air-filled ionization chambers need nearly no maintenance, leakage in N_2 filled chambers is not critical. Ar-filled chambers give very little reason for maintenance.

4.1.1 Calibration and sensitivity of ionization chambers

Note that for comparison and simplicity the sensitivity S_{BLM} [C/rad] of various types of BLMs is calculated for 1 rad dose created by MIPs in the following sections.

The number of electrons (n_e) produced in the gap D of an ionization chamber by one minimum ionizing particle (MIP) is

$$n_e = \frac{D \cdot \rho}{W} \cdot \frac{dE}{dx}$$

with dE/dx from Eq. (1) (Bethe–Bloch)[2], ρ the density of the medium, and W the W value, i.e., the energy to create one electron/ion pair [41]. The valves ρ and W can be collected from text books. Note that W is considerably higher than the usual 'first ionization potential' given in most textbook tables. The valve W is about constant for many gases and radiations.

Example: argon-filled chamber:

$$\rho = 1.661 \cdot 10^{-3}\ \text{g/cm}^3\ (20^\circ\text{C, 1 atm}),\ \mathrm{d}E/\mathrm{d}x = 1.52\ \text{MeV/(g/cm}^2\text{)}$$
$$\Rightarrow n_e \approx\ 100/\text{cm} \cdot D\ \text{[e/MIP]}\ .$$

The intrinsic sensitivity $S_{BLM} = S_{ION}$ (normalized to 1 rad) of an ionization chamber depends on its size. Let us assume as an example a 1 L argon-filled chamber with 100% charge sampling efficiency:

$$S_{\text{Ion}} = 100\frac{\text{erg}}{\text{g}} \cdot \frac{1\text{eV}}{1.6 \cdot 10^{-12}\text{erg}} \cdot \frac{1e^-}{26\text{eV}} \cdot \frac{1.66 \cdot 10^{-3}\text{g}}{\text{cm}^3} \cdot 1000\ \text{cm}^3 \cdot \frac{1.6 \cdot 10^{-19}\text{C}}{e^-} = 638\frac{\text{nC}}{\text{rad}}$$

| 1 rad |·| eV → erg |·| W |·| ρ |·| 1 ltr. |·| e⁻ charge |

This value correlates well with the measured values in the table of Fig. 16. A beneficial characteristic of ion chambers is that their sensitivity is determined by geometry (size), and that the sensitivity is relatively independent of the applied voltage.

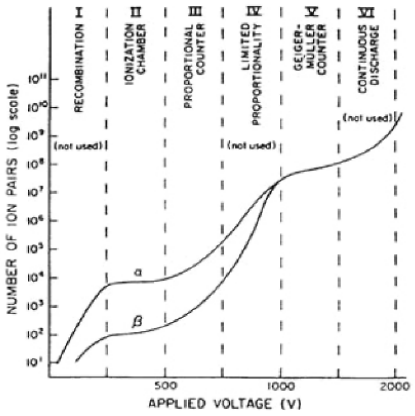

Fig. 14: Regions of gas-filled ionization chambers for α and β particles, from Ref. [31]

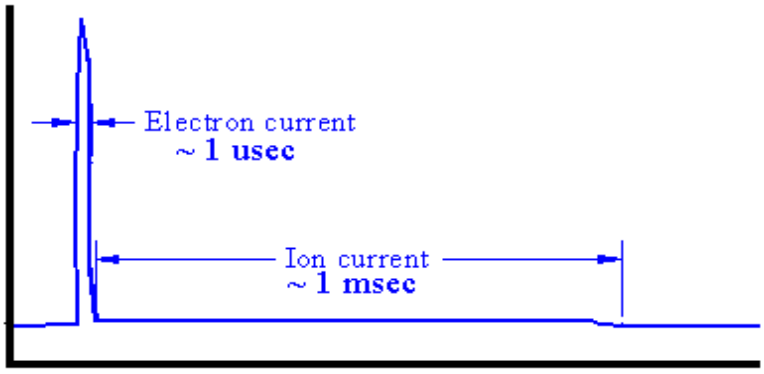

Fig. 15: Typical signal of an ionization chamber, from Ref. [36]

[2] The cross-section for nuclear interaction is about $5 \cdot 10^{-6}$ times the ionization cross-section (10^{-16} cm^2). The cross-section for excitation is about 10^{-17} cm^2. Neither contributes significantly to the energy deposition. Rutherford (nuclear) scattering does not produce significant energy transfer, but angular spread.

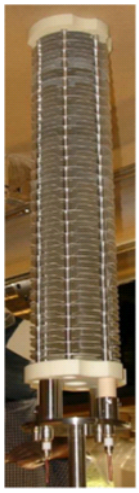

LHC	TEVATRON/RHIC/SNS
T = 0.3 μs (t_{fall} 200μs)	T = 10μs => 3 μs (t_{fall} 560 => 72 μs)
1.5 ltr N_2 at 1.1 bar	0.11 ltr Ar at 1 bar
V = 800 – 1800 V	500 - 3500 V
Dynamic range >10^8 (>10^{-12} – <10^{-3} A)	Dynamic range >10^6 300 pA – 500 μA
Leak current <1 pA	Leak current 10 pA => <100 fA
S: 156 pA/(rad/h) (Cs^{137}) (560 nC/rad)	19.6 pA/(rad/h) (Cs^{137}) (70 nC/rad)
Collection effeciency: >90 %	Collection effeciency: 77% -> 92 %

Fig. 16: Comparison between LHC and SNS ionization chamber (courtesy of B. Dehning and M. Stockner, CERN). For the SNS chamber some improvements from the original Tevatron and RHIC chamber [39, 40] are indicated by '=>'.

4.2 Long ionization chamber

A 'short' ionization chamber described in Section 4.1 covers only a small part of an accelerator; therefore a large number need to be installed to get good coverage. To overcome this problem in linacs or transport lines, a long and gas-filled coaxial cable (e.g. Andrew® HJ4.5-50 HELIAX) can be used as an ionization chamber. In 1963, Panowsky [42] proposed a BLM system for SLAC consisting of one long (3.5 km) hollow coaxial cable. It was an industrial RG-319/U cable with a diameter of 4.1 cm, filled with Ar (95%) + CO_2 (5%). It was named Panowski's long ionization chamber or PLIC. It was mounted on the ceiling along the linac, about 2 m from the beam. This BLM system worked for more than 20 years and was upgraded for the SLC [43]. Nearly the entire SLC is covered by a few PLICs.

Position sensitivity is achieved by reading out at one end the time delay Δt between the direct pulse and the reflected pulse from the other end (see Fig. 17). The time resolution due to the electron collection time of $t_e \approx$ 270 ns and the dispersion in the cable is about 50 ns (~ 15 m) for 6 km long cables, for shorter PLICs about 5 ns (~ 1.5 m) was achieved. This principle of space resolution works for one-shot (or one-turn) accelerators (and transport lines) with a bunch train much shorter than the length of the cable and with relativistic particles. For particles travelling significantly slower than the signal in the cable ($\approx 0.92c$), the resolution of multiple hits in the cable becomes difficult. In this case and for circular machines it is necessary to split the cable. Each segment has to be read out separately, with spatial resolution approximately equal to the length of the unit (see Fig. 18). This was done at various linacs, e.g., ELBE [44] and in the BNL 200 MeV linac [45], but also in some rings, e.g., in the AGS ring, Booster and transport lines [46, 47]. In the KEK-PS, 56 air-filled cables with a length of about 6 m have been installed. Using amplifiers with a variable gain, a dynamic range of 10^4 is achieved [48].

Long ionization chambers made of commercial cables are simple to use, cheap, and have a uniform sensitivity. The isolation is not very radiation hard, nevertheless these cables were used in SLAC for more than 20 years without serious problems.

4.2.1 Calibration and sensitivity of long ionization chambers

The sensitivity S_{long_ion} of a long ionization chamber depends on its geometry and diameter. A sensitivity of

$$S_{\text{long\_ion}} \approx 200 \text{ nC/rad/m}$$

can be expected [49] for a 7/8 inch argon-filled (1 atm) cable. Commercial cables have a typical resistance of $R = 10^{13}$ Ωm between the inner and outer conductor, with a bias of $U = 100$ V this gives a dark current of $I_{\text{dark}} = U/R = 10$ pA/m. For long cables of the order of km, this limits the dynamic range of such a BLM. F. Hornstra [49] proposed a cable with guard electrodes to improve the dark current and therefore its dynamic range.

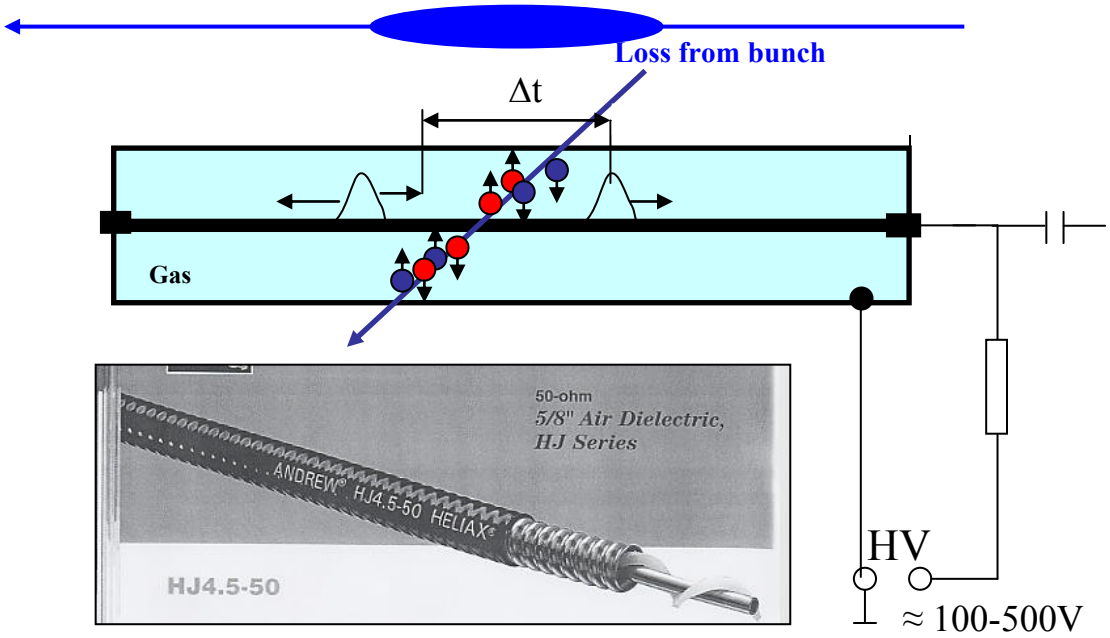

Fig. 17: Principle of position measurement with long ionization chambers. The inset picture is an example of a commercial HELIAX cable.

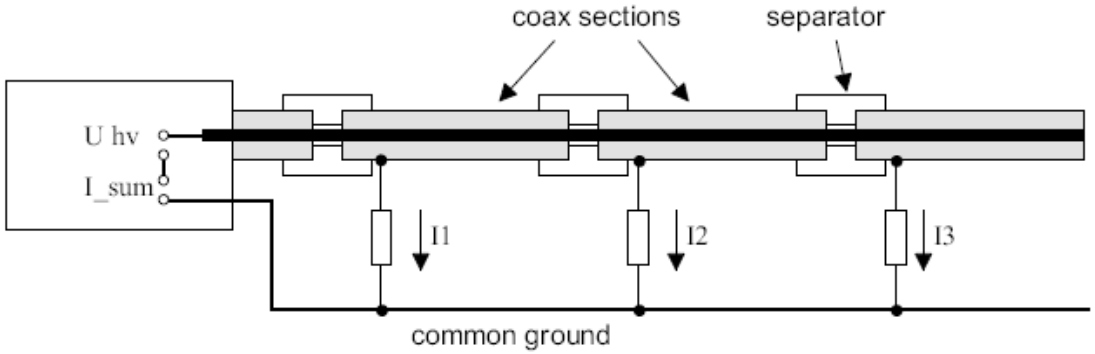

Fig. 18: Principle of a sectioned cable [44]. The signal can be measured at I1, I2, etc.

4.3 Solid-state ion chamber – PIN photodiode

The required energy to create an electron-hole pair in a semiconductor is about 10 times smaller than creating an electron/ion pair in gas. In addition, the density of a semiconductor is about three orders of magnitude larger than for gas (at 1 atm). Therefore a MIP creates in a semiconductor much more signal per path-length than in a gas volume. Let us assume as an example a large-area silicon-PIN photodiode used as a 'solid-state ionization chamber' with an active area $A = 1$ cm^2. Such diodes are commercially available from Hamamatsu (http://www.hamamatsu.com), for example. A MIP creates

free charges in the depletion (or 'intrinsic' or I-) layer between the high doped p^+- (P-) layer and low doped n- (N-) layer of the P-I-N diode (see Fig. 19). The width d of the depletion layer is given by

$$d_{n,p} \approx 0.5 \cdot \sqrt{U\,[\mathrm{V}] \cdot \rho_{n,p}\,[\Omega\mathrm{m}]}\ ,$$

where $\rho_{n,p}$ is the specific resistance of the n- or p- doped silicon and U is the applied bias voltage. Since the low-doped n-layer has a much higher resistance ($\approx$ 5–10·10^3 Ωm) most of the depletion layer is located in the n-layer. Assuming a reversed bias voltage of 25 V, the depletion layer has a width of about 100–200 µm. At about 30–40 V the width d saturates due to the limited thickness of the Si-layers. The energy deposition in Si for a MIP is dE/dx = 3.7 MeV/cm/MIP. The energy to create an electron e (-hole pair) in silicon E_e is only 3.6 eV/e$^-$. Therefore N_e = dE/dx · d/E_e = 1.03 ·10^4 e/MIP are created in a 100 µm depletion layer. The electrons are guided to the n+-layer with an efficiency of >> 80%. The electron mobility μ_e is higher than for gas; typical electron mobility for doped silicon at room temperature (300 K) is

$$\mu_e \approx 0.3\ \mathrm{m}^2/(\mathrm{V \cdot s})$$

(http://www.ioffe.ru/SVA/NSM/Semicond/Si/electric.html); [for holes: $\mu_{hole} \approx$ 450 cm^2/(V·s)]. Owing to the small gap d = 200 µm and a high electric field E = 25 V/200 µm = 1.25 ·10^5 V/m the transit time t_e of the signal is very fast:

$$t_e = d/(\mu_e E) \approx 5.3\ \mathrm{ns}\ .$$

The capacity C of the diode is proportional to A/d and to $1/\sqrt{V}$ and saturates with the width of the depletion layer at around 30 V at values between $C \approx$ 10–100 pF, depending on the area A of the diode. Therefore the rise time of the signal defined by the time constant $\tau = C \cdot R_L$ (R_L = load resistance,) might be in the same order of magnitude: assuming R_L = 50 Ω:

$$\tau = 100\ \mathrm{pF} \cdot 50\ \Omega = 5\ \mathrm{ns}\ .$$

Owing to the finite resistance between the two electrodes (p^+ and n^+) of the diode a dark current of a few nA is typical. The dark current is proportional to the applied bias voltage and does not depend on the thickness of the depletion layer. However, radiation damage (up to 10^6 rad [50]) leads to an increase of the dark current while most of the other parameters remain unchanged.

Note also that not too strong magnetic fields do not influence the charge collection in PIN-diodes. Therefore they can work as BLMs in stray fields of magnets.

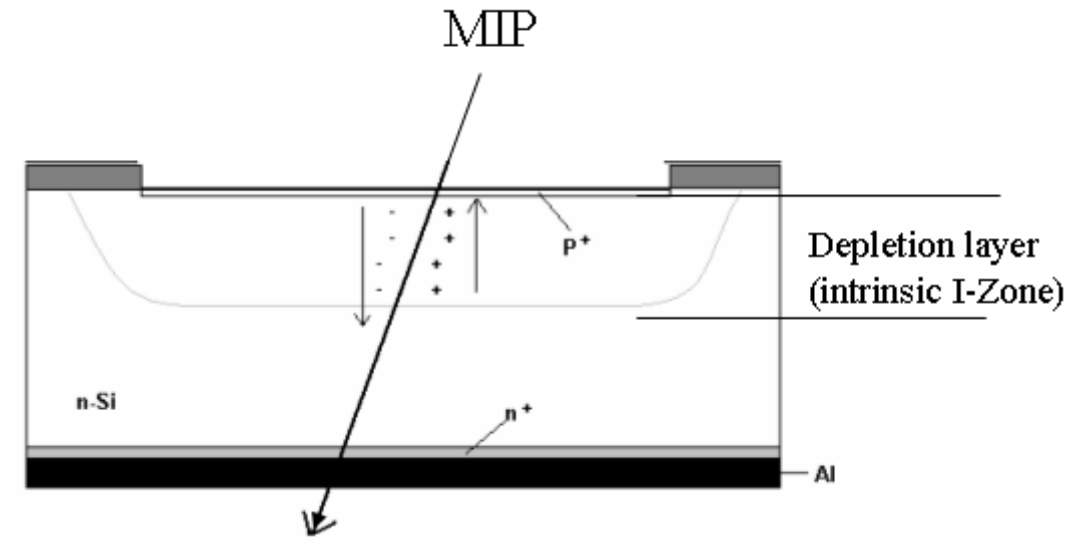

Fig. 19: Schematic of the signal creation in a PIN diode by a MIP

4.3.1 Calibration and sensitivity

The sensitivity S_{PIN} can be calculated with the help of Eq. (2); 1 rad = 3.1 $\cdot 10^7$ MIP/cm^2. Assuming a diode with A = 1 cm^2 and a depletion layer width d = 200 μm, resulting in $N_e = 2 \cdot 10^4$ e/MIP (assuming nearly 100% collection efficiency), we get

$$S_{PIN} = 2 \cdot 10^4 \frac{e}{\text{MIP}} \cdot 3.1 \cdot 10^7 \frac{\text{MIP}}{\text{cm}^2 \cdot \text{rad}} \cdot 1.6 \cdot 10^{-19} \frac{C}{e} = 100 \frac{nC}{\text{rad} \cdot \text{cm}^2}$$

Operating such a diode in a current mode like an ionization chamber the sensitivity is

$$S_{PIN} = 100 \text{ nC/rad}$$

for a 1 cm^2 diode with a depletion layer width of d = 200 μm.

A recent example of a current mode PIN photodiode BLM system can be found in Ref. [51].

4.3.2 Pin diode in counting mode

Circular electron accelerators emit hard synchrotron radiation (SR). The radiation interacts with the BLMs and a separation between SR background and the beam loss distributions using BLMs in current mode technique is difficult to achieve [51]. HERA, for example, was an accelerator with an electron and a proton ring in the same tunnel, operating at the same time. Protection of the superconducting proton magnets from beam-loss-induced quenches must rely on a BLM system which sees only the proton beam losses and not the SR background. The (hadronic) shower created by beam losses includes a large number of charged particles, in contrast to the photons of the SR. The HERA BLM system consists of two PIN photodiodes, mounted close together (face to face) and read out in coincidence [26]. Thus charged particles crossing through the diodes give a coincidence signal, while photons which interact in only one diode do not. In contrast to the charge detection of most other BLM systems, coincidences are counted while the count rate is proportional to the loss rate as long as the number of overlapping coincidences is small. Counting of MIPs crossing both diodes has a few implications:

1) Both channels need a discriminator to suppress dark counts due to noise. Since the signal of one MIP is still weak, the threshold also cuts some of the MIP signals. The efficiency of such a BLM for MIPs has been measured [52, 53]. It was found to be about ε_{count} = 30–35%/MIP for the coincident readout of the BLM which includes also the readout electronics. Assuming a dose-rate of 1 rad/s = 3.1 $\cdot$ 10^7 MIP/s/cm^2 [Eq. (2)] gives a sensitivity of

$$S_{count} = \varepsilon_{count} \cdot 31 \text{ MHz/cm}^2\text{/rad} = 9.3 \text{ MHz/rad}$$

for a diode with A = 1 cm^2.

2) The noise (dark count rate) is very small, typically < 0.01 Hz due to the coincident readout.

3) The detector cannot distinguish between one or more MIPs crossing both diodes at the same time. The shortest signal length is defined by the response time of the diodes, but in practice it is defined by the readout electronics. An efficient counting type of BLM should have a signal length shorter than the bunch distance, so that the maximum measured loss rate is the bunch repetition rate of the accelerator (at HERA 10.4 MHz). Saturation effects occur even before the maximum rate but they can be corrected by applying Poisson statistics [54].

4) The dynamic range lies between the dark count rate of < 0.01 Hz and the maximum rate (e.g., HERA: 10.4 MHz) and might reach 10^9 [55]. However, background counts from synchrotron radiation have to be taken into account.

Two effects contribute to the background rate:

a) A high energy photo- or Compton-electron produced by a SR photon conversion in the first diode can reach the other diode and creates a coincident signal in the two diodes. One can find in Ref. [56] a detailed description of how a copper inlay between the two diodes reduces the probability of background counts due to photo- or Compton electrons. The efficiency of the BLM to beam losses is not changed by this inlay.

b) The high photon rate of SR gives a higher probability for the coincident conversion of two photons in the two diodes. An efficiency of the BLM of $\varepsilon_\gamma = 3.5 \cdot 10^{-5}$ was measured [57, 58] which is already four orders of magnitude below the MIP efficiency. A reduction of the high photon flux by a lead hat helps in two ways [58]. First the probability for a coincident conversion of two photons is additionally reduced and secondly the background rate of photo- or Compton-electrons is reduced.

The PIN diode BLM system (Fig. 20) at HERA was successfully operated between 1992 and 2007 without significant problems or radiation damage.

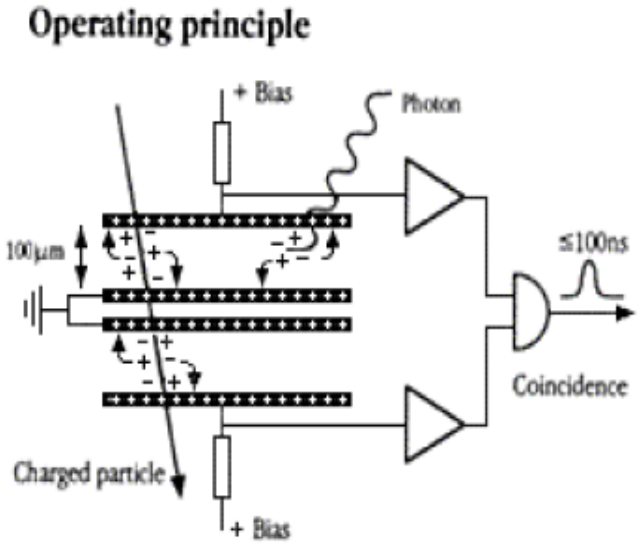

Fig. 20: Operating principle of counting mode PIN diode BLM, from Ref. [59]

4.4 Secondary emission monitors

Ionization chambers have the disadvantage of being slower than the bunch distance in most accelerators (except for PIN diodes in current mode). Counting mode devices have to integrate the counts over a lot of bunches to get a statistically relevant signal. A simple, robust and cheap BLM is a secondary emission chamber. As described in Section 3.2, secondary electrons are emitted from a surface due to the impact of charged particles. An efficiency of a few per cent was measured for many metal surfaces (Fig. 12). That means that 100 MIPs crossing an area will produce only a few electrons. Since Secondary Electron Emission (SEM) is a very fast effect, such a monitor is very fast (≈ ns). But its very low sensitivity makes it useable only in high radiation fields; with the additional advantage that it consists of nothing more than a few layers of metal (see Fig. 21). Therefore it is a very radiation hard monitor. The monitor has to be evacuated to avoid contamination of the signal due to gas ionization. Since the efficiency of gas ionization is much higher, a gas pressure of better than 10^{-4} mbar should be achieved to get < 1% signal from ionization. Especially in high radiation fields, gas ionization will lead to nonlinearities while SEM is a very linear process over a wide range of intensities [22, 23]. Unavoidable ionization outside the detector at the feedthroughs and connectors limits the linearity at the lower end of the signal [38].

A SEM multiplier extends the use of SEM BLMs to small radiation intensities. As far back as 1971 CERN [60] used Aluminium Cathode Electron Multipliers (ACEM) for beam loss measurements. This device is a photomultiplier tube where the photocathode is replaced by a simple aluminium cathode. The SEM electrons are guided to dynodes where they are amplified; amplifications up to 10^6 were possible. An example for recent use of ACEMs can be found at FLASH [61, 62].

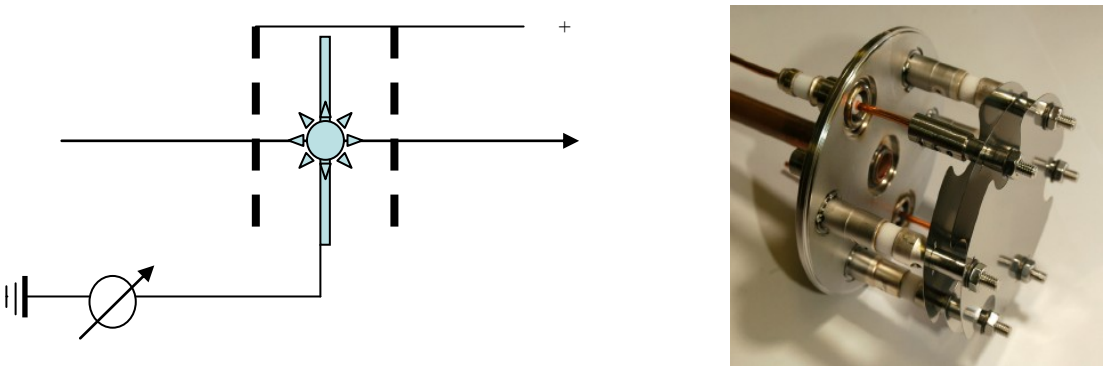

Fig. 21: Left: a sketch of a SEM monitor. The SEM foil in the middle is surrounded by positive charged grids to avoid the repulsion of the emitted SEM electrons. Right: LHC SEM BLM with gas sealed cover removed [from Ref. 60]. A NEG ST707 foil keeps the gas pressure below 10^{-4} mbar.

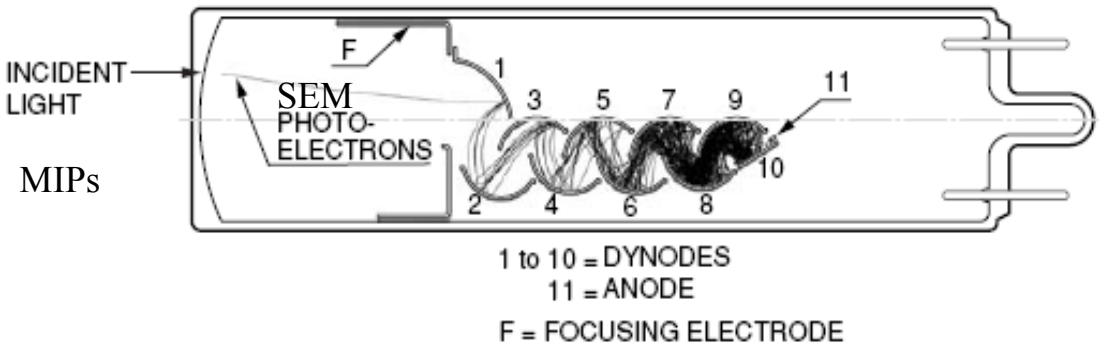

Fig. 22: Sketch of an aluminium electron multiplier [63]

4.4.1 Calibration and sensitivity

SEM chambers can be built in any size. Let us assume a SEM yield of μ_{SEM} = 5% = 0.05 e/MIP (from Ref. [23]). With Eq. (2) this gives

$$S_{\mathrm{SEM}} = 3.1 \cdot 10^{7} \frac{\mathrm{MIPs}}{\mathrm{cm}^2\,\mathrm{rad}} \cdot 0.05 \frac{e}{\mathrm{MIP}} \cdot 1.6 \cdot 10^{-19} \frac{\mathrm{C}}{\mathrm{e}} = 0.25 \frac{\mathrm{pC}}{\mathrm{rad\,cm}^2}$$

The gain of the ACEM tube can be adjusted by the applied high voltage and varied by a few orders of magnitude. This has to be taken into account. Let us take as an example the diameter of the ACEM Type 8941, which has an area of A = 8 cm^2. Therefore the sensitivity S for this BLM can be written as

$$S_{\mathrm{ACEM}} = 2 \frac{\mathrm{pC}}{\mathrm{rad}} \cdot \left(\mathrm{ACEM}_{\mathrm{gain}}\right)$$

Since the gain may drift as with a photomultiplier tube, care has to be taken to keep the high voltage and the gain stable. Also radiation damage in ACEMs may lead to a reduction of the gain (not reported up to now).

4.5 Scintillation detectors

SEM-based BLMs are very fast but still have a moderate sensitivity. An equivalent speed but much higher sensitivity can be expected from scintillation counters. This is a combination of a scintillating material and a photomultiplier tube (PMT). Large-area plastic (organic) and liquid scintillators are available. Plastic scintillators, in particular, can be modulated in nearly any kind of shape and size while inorganic scintillators are expensive and limited in size. Descriptions of how the scintillation process works can be found in Ref. [31] and in various text books, e.g., Refs. [33, 34]. One important fact should be stressed here: *Note that the flux density of photons from the scintillator into the light guide is 'incompressible'! The cross section of the scintillator should not be larger than the cross section of the light guide.* However, large scintillators can be useful to enhance the solid angle of beam loss detection if the resulting radiation is not uniformly distributed. This is often true if the BLM is located very close to the beam pipe where the radiation is peaked into a solid angle. Examples are shown in Fig. 23. Typically a thin layer of scintillator (1–3 cm) is sufficient to ensure sensitive loss detection.

The light L produced by a charged particle in a scintillator is for small dE/dx (e.g., for MIPs): $dL/dx = R_s\, dE/dx$, where R_s is the ratio of the average number of emitted photons to the energy of the incident radiation absorbed by the scintillator. The ratio R_s is tabled for typical scintillator materials by various commercial suppliers, e.g., Ref. [64]. For a typical plastic scintillator, e.g., NE102A, one needs energy to create one photon of $1/R_s \approx 100$ eV/photon. The scintillation light is then transported from the scintillator layers to the photosensitive device via light guides. Attenuation occurs due to internal absorption and mainly due to missing internal multiple reflections. The light is reflected at the surface of the scintillator and the light guide due to their higher refraction coefficient n_1. Once the angle of the light relative to the surface is larger than the the critical angle given by $\Theta_c = \arcsin(n_2/n_1)$ ($n_2/n_1 \leq 1$, n_2 = refractive index of the less dense medium, here air $n_2 = 1$) the light leaves the material. A reflective foil, e.g., aluminium foil or with paper, reflects the light back, but with some higher absorbtion. Note that the main process of the light transport is still the internal total reflection defined by the higher refration index. Any distortion will lower the light transport efficiency. A good matching between the light guide and the PMT is also very useful. Therefore:

1) Match the size of the light guide and the photocathode.
2) Optical grease between the light guide and the PMT helps to couple out the light

A carefully designed scintillator assembly has an overall collection efficiency of about $\varepsilon_{coll} \approx 60\%$.

3) The emission spectrum of the scintillator and the spectral response of the PMT should match.

Well-matched spectra result in a photon-to-photoelectron conversion efficiency of the photocathode of $\varepsilon_{cath} \approx 30\% = 0.3$ e/photon. These photoelectrons are amplified in the PMT with a gain between $10^5 \leq PMT_{gain} \leq 10^8$, depending on the type of PMT and the applied high voltage. The shape of the scintillation pulse is characterized by a fast rise time of the order of 1 ns and a decay time of a few ns [65].

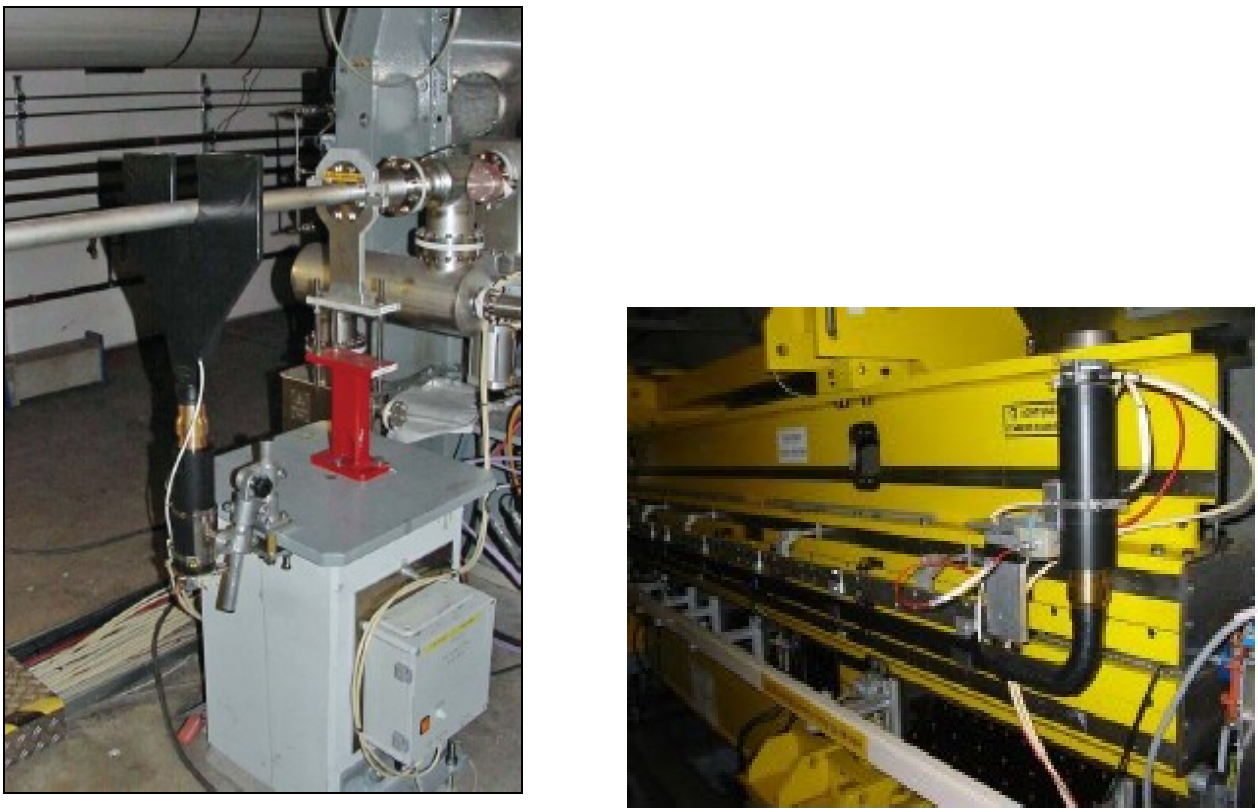

Fig. 23: Scintillator BLMs at FLASH (DESY); Left: Surrounding the beam pipe; Right: Long scintillator along an undulator. Courtesy L. Fröhlich, DESY.

4.5.1 Calibration and sensitivity of scintillation counters

Since the sensitivity depends on the type and size of the scintillator, let us assume a material of NE102A. NE102 has a density ρ = 1.032 g/cm^3 (weight = 1032 g/L.) and a light output of R_s = 0.01 photon/eV. A deposition of 1 rad = 100 erg/g into this volume creates N number of photons:

$$N = \frac{100\text{erg}}{\text{g}\cdot\text{rad}} \cdot 1032\frac{\text{g}}{\text{L}} \cdot \frac{1\text{eV}}{1.6\cdot 10^{-12}\,\text{erg}} \cdot R_s \approx 6.5\cdot 10^{14}\,\frac{\text{photons}}{\text{rad}\,\text{L}}$$

Therefore the sensitivity S_{scint} for Ne102A scintillator is

$$\boxed{S_{\text{scint}} = 6.5\cdot 10^{14}\,\frac{\text{photons}}{\text{rad}} \cdot \varepsilon_{\text{coll}} \cdot \varepsilon_{\text{cath}} \left[\frac{\text{electrons}}{\text{photon}}\right] \cdot \frac{1.6\cdot 10^{-19}\text{C}}{\text{electron}} \approx 18\frac{\mu\text{C}}{\text{rad}\,\text{L}}}$$

Assuming a counter with a volume of V = 1 L = 1000 cm^3 (the dimension might be 25·25·2 cm^3) connected to a PMT this gives a sensitivity S_{scint}:

$$\boxed{S_{\text{scint}} = 18\frac{\mu\text{C}}{\text{rad}} \cdot \text{PMT}_{\text{gain}}}$$

Note that the light transmission through the scintillator (and the Plexiglas light guide, $\varepsilon_{\text{coll}}$) changes on account of radiation damage. This depends strongly on the scintillator material, but for organic scintillators a typical value can be assumed: the transmission decrease to 1/e of its original value happens after about 0.01–1 MGy (1–100 Mrad) collected dose. Liquid scintillators are somewhat radiation harder and have about the same sensitivity. An older example of liquid scintillator BLMs can be found in Ref. [66]. Complete liquid scintillator detectors are also commercially available [64]. Note

that inorganic scintillators like BGO or CsJ(Tl) have about a factor 10–50 higher sensitivity due to their higher density (factor ≈ 5) and larger R_s (factor ≈ 5). But their radiation hardness is poor and large-sized crystals are very expensive.

The gain of the same type of photomultipliers (PMT_{gain}) varies within a factor of 10. Therefore a careful inter-calibration of the BLM sensitivities is necessary by adjusting the high voltage (HV). The drift of the gain is a well known behaviour of PMTs. A stabilized HV source and continuous monitoring of the photomultiplier gain over the run period are necessary to keep the calibration error small.

4.6 Cherenkov light

Scintillation detectors are sensitive to charged particles *and* to X-rays. A Cherenkov detector is nearly not sensitive to X-rays because the Cherenkov effect occurs only when the velocity of a *charged* particle traversing a dielectric medium is faster than the speed of light in that medium. In that case photons are emitted at an angle with respect to the trajectory of the particle defined by the velocity β of the particle and the refraction index *n* of the medium. The light can be focused on a PMT to build a BLM (see Fig. 24). The Cherenkov material (e.g., synthetic fused silica) has good radiation hardness up to about 1 MGy [67]. An example for a Cherenkov based BLM system can be found in Ref. [68].

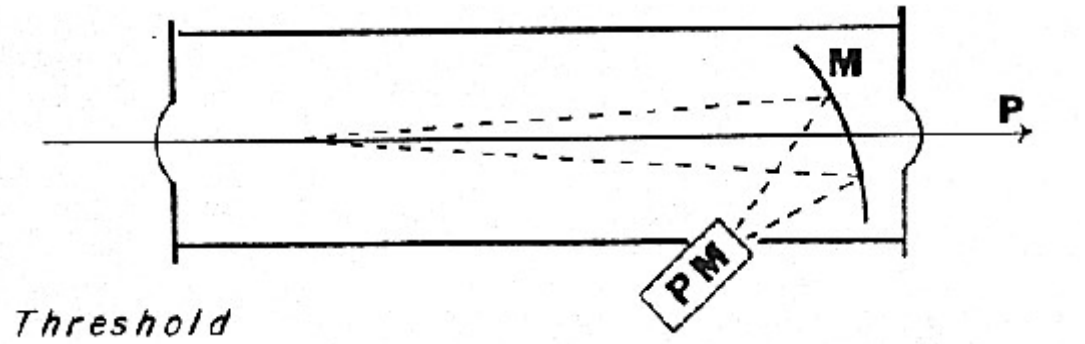

Fig 24: Sketch of a typical Cherenkov detector. M = mirror, P = charged particle, PM = photomultiplier.

4.6.1 Calibration and sensitivity

The photon yield d*N*/d*x* is defined for the Cherenkov effect:

$$\text{photonyield:}\quad \frac{\mathrm{d}N}{\mathrm{d}x} = 2\cdot\pi\cdot\alpha\cdot\sin^2\Theta\cdot\left(\frac{1}{\lambda_1}-\frac{1}{\lambda_2}\right)$$

with: $\cos\Theta = 1/(\beta\cdot n)$, $\beta > 1/n$, $\alpha = 1/137.036$ and $\lambda_{1,2}$ = wavelength interval.

A typical photocathode is sensitive between $\lambda_1 = 350 \le \lambda \le \lambda_2 = 500$ nm. Therefore:

$$\frac{\mathrm{d}N}{\mathrm{d}x} = 390\cdot\sin^2\Theta\,\frac{\text{photons}}{\text{cm}}\,.$$

As pointed out in the beginning, let us assume that the radiation is created by MIPs which have β = 1. Fused silica has a refraction index of $n = 1.55$, therefore $\Theta = 49.80$ and

$$\mathrm{d}N/\mathrm{d}x = 227 \text{ photons/(MIP cm)}\,.$$

A 1 L Cherenkov detector ($10\cdot10\cdot10$ cm^3) produces [(Eq. 2)]:

$$\frac{3.1\cdot10^{7}\,\mathrm{MIP}}{\mathrm{cm}^{2}\cdot\mathrm{rad}}\cdot\frac{227\mathrm{photons}}{\mathrm{MIP}\cdot\mathrm{cm}}\cdot1000\,\mathrm{cm}^{3}=7\cdot10^{12}\,\frac{\mathrm{photons}}{\mathrm{rad}}$$

The collection efficiency of the Cherenkov light is in the order of ε_{coll} = 80%, which is valid only for directed light created by particles crossing the detector with a common and know angle. This might not be true for beam loss monitoring (Monte Carlo simulation needed). The collected light is then converted into photoelectrons at the photocathode of the PMT with an efficiency of about ε_{cath} = 30%. The sensitivity S_{Che} for a 1 L Cherenkov detector connected to a PMT can be calculated by

$$S_{\mathrm{Che}}=7\cdot10^{12}\,\frac{\mathrm{photons}}{\mathrm{rad}}\cdot\varepsilon_{\mathrm{coll}}\cdot\varepsilon_{\mathrm{cath}}\cdot\frac{1.6\cdot10^{-19}C}{e^{-}}\cdot\mathrm{PMT}_{\mathrm{gain}}=270\frac{\mathrm{nC}}{\mathrm{rad}}\cdot\mathrm{PMT}_{\mathrm{gain}}$$

This is only a factor 2–3 smaller than a 1 L ionization chamber but the response time of a Cherenkov detector is much faster. It is like a scintillator counter defined by the response time of the PMT of < 10 ns. But note again that the calculated sensitivity S_{Che} is valid only for directed light owing to the 80% collection efficiency.

Since a very efficient Cherenkov detector needs good mirrors, it might become expensive and its maintenance might become costly. A very cheap Cherenkov BLM was developed at CEBAF using only a simple and cheap PMT [69]. The Cherenkov light is created in the glass tube of the PMT which is then directly detected. The housing of the PMT was made of simple water pipes (see Fig. 25). It is a quite radiation tolerant system; however the darkening of the PMT glass has to be compensated by increasing the PMT gain. Such a system is not sensitive enough to measure 'small normal' losses but it was used to control and limit strong and dangerous losses.

The stabilization of the PMT gain, as discussed in Section 4.5.1, is also valid in the case of Cherenkov detectors.

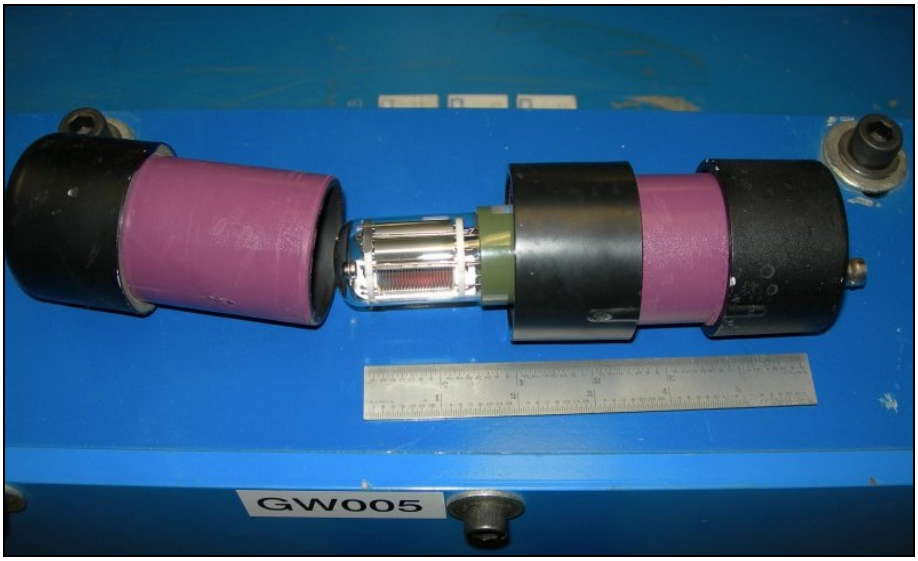

Fig. 25: The simple CEBAF Cherenkov BLMs. Courtesy K. Jordan.

4.6.2 Optical fibres

Another idea for reducing the costs of a BLM system is to reduce the quantity of BLMs but with sufficient covering of the accelerator. One can use Cherenkov light created in long optical fibres to determine the position of beam losses. It allows real-time monitoring of loss location and loss intensity

like in PLICs (Section 4.2). The fast response of the Cherenkov signal is detected with photomultipliers at the end of the irradiated fibres. A time measurement provides the position measurement along the fibre while the integrated light gives the amount of losses (see Fig. 26). A longitudinal position resolution of 20 cm (= 1 ns at $v = 0.66c$) is possible. The use of high purity quartz fibres (suprasil) has some advantages:

- Only Cherenkov emission, no scintillation
- $n = 1.457$, high refraction index
- withstands $30 \cdot 10^9$ rad, radiation hard

Scintillating fibres give about 1000 times more light output but are much more sensitive to radiation damage (reduction of 1/e at $\approx 10^8$ rad) [71].

There are two major issues to address when considering the sensitivity of BLMs using the Cherenkov effect in single quartz optical fibres.

- The light yield caused by the passage of a single charged particle in a fibre.
- The probability of survival of the emitted photons.

The Cherenkov cone for $\beta = 1$ particles (MIPs) is $\Theta \approx 47^{\circ}$.

The condition for light capture and transport down the fibre is given by:

$$\xi \geq \arcsin\left(\frac{n_{\text{clad}}}{n_{\text{core}}}\right),$$

where ξ depends on (shower) particle trajectory. The numerical aperture NA is defined as:

$$\sqrt{n_{\text{core}}^2 - n_{\text{clad}}^2} = NA \approx 0.3 .$$

The distribution of photons trapped inside a fibre as a function of the impacting particle's angle a and impact parameter b. For more details see Figs. 27, 28 and Ref. [72]. Since the efficiency of Cherenkov fibres depends so strongly on the impact distance and angle, a general formula for the sensitivity of Cherenkov fibre BLMs cannot be given here. Monte Carlo simulations are necessary to calculate the response at certain conditions.

Examples for Cherenkov fibre based BLM systems can be found in Refs. [73, 74]. Also dose measurements can be done by optical fibres, but they are not treated here because of their long time response of hours or days [75].

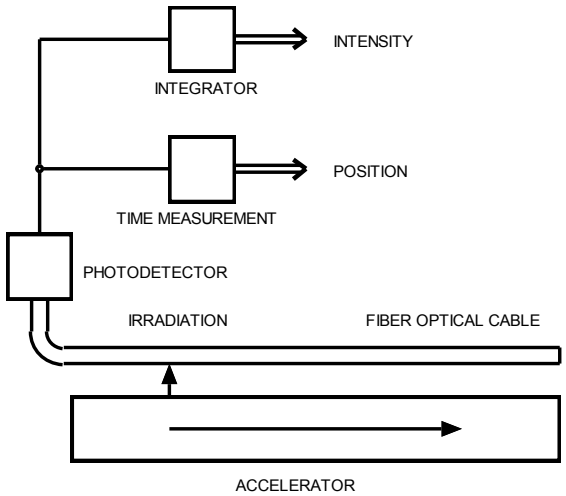

Fig. 26: Schematic of the detection of irradiation by means of an optical fibre; from Ref. [70]

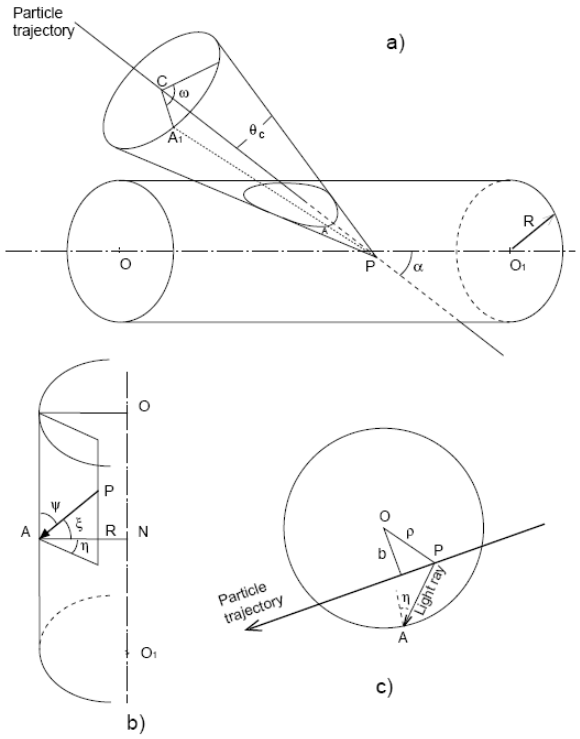

Fig. 27: A schematic view of the Cherenkov effect in a step index optical fibre. A photon emitted at the point P travels along the Cherenkov cone and hits the interface core-cladding at point A. (a) Three-dimensional view; (b) Blow-up view of the point of impact of a light ray on the interface core-cladding; (c) Projection into a plane perpendicular to the fibre axis. From Ref. [72].

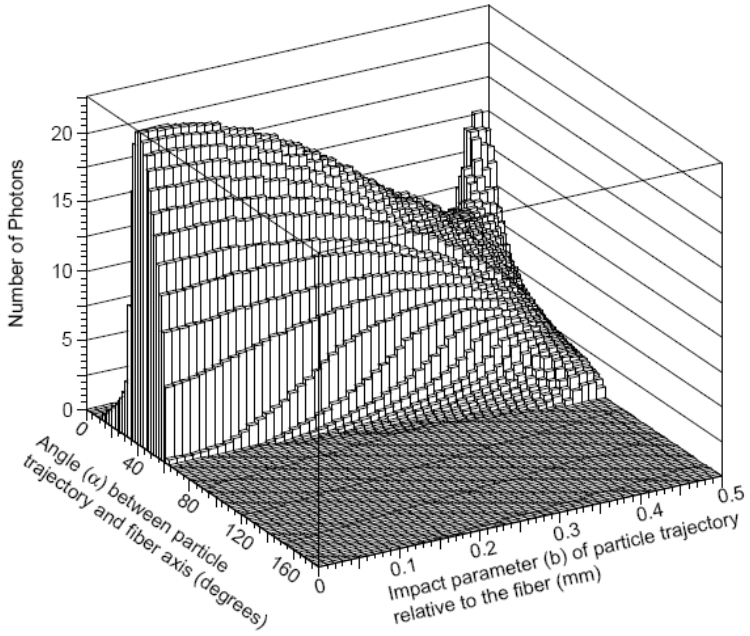

Fig. 28: The distribution of photons trapped inside a fibre as a function of the impacting particle's angle *a* and impact parameter *b*. *NA* = 0.37. From Ref. [72].

5 Summary

Different types of beam losses together with some examples were shown. Beam loss monitoring techniques for measuring losses along an entire accelerator have been discussed with the focus on the sensitivity of the various types.

The most common BLM is a short ionization chamber. Whether a simple air filled chamber is adequate, or an argon or helium filled chamber with superior higher dynamic range must be used, depends on the conditions of the particular accelerator. Ionization chambers are radiation resistant but respond to synchrotron radiation.

Long ionization chambers using a single coaxial cable work well for one-shot accelerators or transport lines. To achieve spatial resolution of losses along an entire accelerator two conditions must be fulfilled: 1) The machine must be much longer than the bunch train and 2) the particles must be relativistic, or 3) the long chamber has to be split into short parts which are read out individually.

PIN diodes with thick depletion layers can be used as 'solid state' ionization chambers. They have a high sensitivity but they exist only in small sizes. The combination of two PIN photodiodes in a coincidence counting mode results in a detector with very large dynamic range and extremely effective rejection of synchrotron radiation. The measured radiation resistance permits long term use also in high energy electron machines with a high radiation background. A limitation is the inability to distinguish overlapping counts, so that the response is linear only for losses which are less than one count per coincidence interval.

A very sensitive system for measuring beam losses is a PMT in combination with a scintillator. Because of the adjustable gain the dynamic range can be large, but the calibration of each device must be adjusted and monitored over time. These systems are also sensitive to synchrotron radiation and are relatively expensive.

Cherenkov counters are insensitive to synchrotron radiation background but they are less sensitive to beam losses. However, with the additional gain of a PMT their sensitivity exceeds the ionization chamber. Long optical fibres can be used like long ionization chambers with the same limitations in the bunch repetition rate. Cherenkov based fibres are much more radiation hard but much less sensitive to losses than scintillating fibres.

The following table summarizes the estimated sensitivity of the BLM types discussed together with some interesting numbers. Note that the estimated sensitivity is true for doses created by MIPs only. Careful Monte Carlo studies are necessary to get the real response of a BLM at its location. A detailed understanding of the reasons for beam losses is most helpful to get the right starting point for the simulation, e.g., where a beam loss might occur.

Detector material	Energy to create one electron [eV/e]	Number of [e / (cm MIP)] (depends on dE/dx and density)	Sensitivity *S* (for MIPs) [nC/rad]
Plastic scintillator	250–2500	10^3– 10^4	≈ $18 \cdot 10^3$ (·PMT_{gain}) (1 ltr.)
Inorganic scint	50–250	10^4–10^5	≈ $200 \cdot 10^3$ (·PMT_{gain}) (1 L)
Gas ionization	22–95	≈ 100 (Ar,1 atm., 20°C)	≈ 600 (·$Elec_{gain}$) (1 L)
Semiconductor (Si)	3.6	10^6	≈ 100 (·$Elec_{gain}$) (1 cm^2 PIN diode)
Secondary emission	2–5%/MIP (surface only)	0.02–0.05 e/MIP	≈ $2 \cdot 10^{-3}$ (·PMT_{gain}) (8 cm^2)
Cherenkov light	10^5–10^6	≈ 10 (H_2O)	≈ 270 (·PMT_{gain}) (1 L)

Acknowledgements

Many thanks to my colleagues Mark Lomperski, Lars Fröhlich, and Gero Kube from DESY for adding a lot of useful hints and comments to this manuscript. Many authors listed in the references provided me with their talks, pictures or data, which is gratefully acknowledged.

References

[1] K. Wittenburg, Beam loss monitoring and control, *Proc. 8th European Particle Accelerator Conference*, EPAC02, La Villette – Paris, 3–7 June 2002.

[2] K. Wittenburg, Beam loss and machine protection, *Proc. 33rd ICFA Workshop*, Bensheim, Germany, 18–22 Oct. 2004.

[3] R.E. Shafer *et al*., The Tevatron beam position and beam loss monitoring systems, Fermilab-Conf.-83-112-E, 1988, *Proc. 12th Int. Conf. on High Energy Accelerators*, pp. 609–615.

[4] B. Holzer *et al*., Beam loss monitoring system for the LHC, CERN-AB-2006-009 and *IEEE Nuclear Science Symposium and Medical Imaging Conference,* El Conquistador Resort, Puerto Rico, 23–29 Oct 2005, IEEE, Vol. 2, pp. 1052–1056.

[5] H. Nakagawa *et al*., Beam-loss monitoring system with free-air ionization chambers, *Nucl. Instrum. Methods* **A174** (1980) 401–409.

[6] P. Thompson *et al*., RHIC beam loss monitor system commissioning year 00 run, *Proc. 9th Beam Instrumentation Workshop*, BIW2000, Cambridge, MA, May 8–11, 2000 and http://www.rhichome.bnl.gov/RHIC/YearZero/early_beam.html.

[7] D.R.C. Kelly *et al*., On the electron beam lifetime problem in HERA, *Proc. 16th IEEE Particle Accelerator Conference*, PAC '95, Dallas, TX, USA, 1–5 May 1995.

[8] N.V. Mokhov *et al*., Beam-induced damage to the Tevatron components and what has been done about it, *Proc. 39th ICFA Advanced Beam Dynamics Workshop 'High Intensity High Brightness Hadron Beams'*, HB2006, Tsukuba City, Japan, 29 May–2 June, 2006.

[9] P. Michel, Strahlverlustmonitore für ELBE, *Strahlungsquelle ELBE*; ELBE-Palaver; http://www.fz-rossendorf.de/FWQ/

[10] J. Hinkson, ALS beam instrumentation: beam loss monitoring, February 1999, not published.

[11] P. Kuske, Accelerator physics experiments with beam loss monitors at BESSY, *Proc. 5th European Workshop on Diagnostics and Beam Instrumentation*, DIPAC01, Grenoble, France, 2001.

[12] C. Steier, J. Byrd and P. Kuske, Energy calibration of the electron beam of the ALS using resonant depolarisation, *Proc. 7th European Particle Accelerator Conference*, EPAC2000, Vienna, Austria, 2000.
[13] K. Wittenburg, Halo and bunch purity monitoring, these proceedings: CAS 2008, Beam Diagnostics, Le Normont, Dourdan, France, 28 May–6 June 2008.
[14] H. Burkhardt, I. Reichel and G. Roy, Transverse beam tails due to inelastic scattering, CERN-SL-99-068.
[15] O. Brüning *et al*., Measuring the effect of an external tune modulation on the particle diffusion in the proton storage ring of HERA, DESY-HERA-94-01, Jan 1994.
[16] K.H. Mess and M. Seidel, Measurement of proton beam oscillations at low frequencies, *Proc. 4th European Particle Accelerator Conference*, EPAC 94, London, 1994, Vol. 2, pp. 1731–1733, and Hamburg DESY Int. Rep. M-94-03-R.
[17] P. Kuske, Accelerator physics experiments with beam loss monitors at BESSY, *Proc. 5th European Workshop on Diagnostics and Beam Instrumentation*, Grenoble, France, 2001.
[18] K.T. Hsu, Real-time beam loss monitoring system and its applications in SRRC, *Proc. 17th IEEE Particle Accelerator Conference*, PAC97, Vancouver, B.C., Canada, 12–16 May 1997.
[19] R.E. Shafer, A tutorial on beam loss monitoring, *Proc. 10th Beam Instrumentation Workshop*, Brookhaven, May 2002.
[20] EGS: http://rcwww.kek.jp/research/egs/index.html, Fluka: http://www.fluka.org/, Geant4: http://geant4.web.cern.ch/geant4/.
[21] E.J. Sternglass, Sci. Pap. 1772, Westinghouse Research Laboratory, Pittsburgh, PA (1954).
[22] E.J. Sternglass, Theory of secondary electron emission by high-speed ions, *Phys. Rev*. **108** (1957) 1.
[23] D. Kramer *et al*., Secondary electron emission beam loss monitor for LHC, *Proc. 8th European Workshop on Diagnostics and Beam Instrumentation*, DIPAC 2007, Venice, 20–23 May 2007.
[24] H.-D. Gräf *et al*., Compton diodes as diagnostic tools in accelerator operation, *Nucl. Instrum. Methods Phys. Res.* **A512** (2003) 453–458.
[25] O. Kaul, B. Sarau and K. Wittenburg, Fast measurement of lifetime changes and beam losses in DORIS by the use of bremsstrahlung from a collimator, *Proc. 3rd European Workshop on Diagnostics and Beam Instrumentation*, DIPAC97, Frascati (Rome), Italy, 1997.
[26] K. Wittenburg, The pin-diode beam loss monitor system at HERA, *Proc. 9th Beam Instrumentation Workshop,* BIW2000, Cambridge, MA, 2000.
[27] A. Arauzo *et al*., LHC beam loss monitors, *Proc. 5th European Workshop on Diagnostics and Beam Instrumentation*, Grenoble, France, 2001.
[28] M. Stockner, *Beam Loss Calibration Studies for High Energy Proton Accelerators* (TU, Wien and CERN, Geneva, 2007) [CERN–THESIS–2008–099].
[29] L. Yuxiong *et al*., The beam loss monitoring system for the HLS storage ring, *Nucl. Instrum. Methods Phys. Res*. **A467–468** (2001) 80–83.
[30] F. Ridoutt and K. Wittenburg, Experience with the electron and proton beam loss monitor system at HERA, *Proc. 5th European Particle Accelerator Conference*, EPAC'96, Sitges, Barcelona, 1996.
[31] C. Leroy, Review of radiation detectors, *Proc. 4th International Summer School and Workshop on Nuclear Physics Methods and Accelerators in Biology and Medicine*, Prague, *AIP Conf. Proc*. **958** (2007), 92–100.
[32] K. Wittenburg, Beam loss detection, *Proc. 1st European Workshop on Diagnostics and Beam Instrumentation*, DIPAC93, Montreux, Switzerland, 3–5 May, 1993, CERN PS/93–35 (BD).
[33] W.R. Leo, *Techniques for Nuclear and Particle Physics Experiments* (Springer, Berlin, 1987), ISBN 3-540-17386-2.
[34] R.C. Fernow, *Introduction to Experimental Particle Physics* (Cambridge University Press, 1986), ISBN-10: 0521379407.

[35] D. Gassner and R.L. Witkover, Design and testing of the new ion chamber loss monitor for SNS, *Proc. 2003 Particle Accelerator Conference*, Portland, Oregon, 2003.
[36] D. Gassner and R.L. Witkover, SNS beam loss monitor system, Slides from http://www.bnl.gov/cad/sns/jennytest1/doc/04-05-2001/ctls%20-5-01.ppt.
[37] B. Dehning *et al*., Measurements and simulations of ionization chamber signals in mixed radiation fields for the LHC BLM system, CERN-AB-2006-086, 2006.
[38] B. Dehning *et al*., The LHC beam loss measurement system, *Proc. 22nd Particle Accelerator Conference* (PAC'07), Albuquerque, NM, 2007.
[39] R.E. Shafer *et al*., The Tevatron beam position and beam loss monitoring systems, *Proc. 12th Int. Conf. on High Energy Accelerators*, Batavia, IL, 1983, pp. 609–615.
[40] R.L. Witkover, E. Zitvogel and R. Michnoff, RHIC beam loss monitor system design, *Proc. 17th Particle Accelerator Conference*, PAC97, Vancouver, B.C., Canada, 1997.
[41] *Average Energy Required to Produce an Ion Pair*, International Commission on Radiation Units and Measurements, ICRU Report 31, Washington D.C. (1979).
[42] W.K.H. Panowski, The use of a long co-axial ion chamber along the accelerator, SLAC-TN-63-57 (1963).
[43] J. Rolfe *et al*., Long ion chamber system for the SLC, SLAC-PUB-4925 (1989).
[44] P. Michel *et al*., Beam loss monitoring with long ionization chambers at ELBE, a beam loss monitor with longitudinal resolution, Radiation Source ELBE Annual Report 2002, FZR-375 April 2003; P. Michel *et al*., Beam loss detection at radiation source ELBE, *Proc. 6th European Workshop on Diagnostics and Beam Instrumentation*, DIPAC 2003, Mainz, Germany, 2003.
[45] J. Balsamo *et al*., Long radiation detector system for beam loss monitoring, *IEEE Trans. Nucl. Sci*. **NS-24** (1977) 1807–1809.
[46] E.R. Beadle *et al*., The AGS beam loss monitor system, *Proc. 1991 IEEE Particle Accelerator Conference*, San Francisco, CA, 1991, pp. 1231–1233.
[47] G.W. Bennett *et al*., The upgraded ring loss radiation monitoring system at the AGS, *Proc. 1989 IEEE Particle Accelerator Conference*, Chicago, IL, 1989, BNL-41824.
[48] N. Nahagawa *et al*., Beam loss monitoring system with free - air ionisation chambers, *Nucl. Instrum.* Methods **174** (1980) 401–409.
[49] F. Hornstra, Improved spirally insulated cable for coaxial ionization chambers, DESY-HERA-89–05, 1989.
[50] K. Wittenburg, Radiation damage in pin photodiodes, *Nucl. Instrum. Methods* **A270** (1988) 56–61 and DESY 87–070 (July 1987), 18 p. and http://www.microsemi.com/brochures/pindiodes/appendix%20f.pdf.
[51] Y. Shimosaki *et al*., Development of beam loss monitor for the SPring-8 storage ring, *Proc. 11th European Particle Accelerator Conference*, EPAC'08, Genoa, Italy, 2008.
[52] F. Ridoutt, Das Ansprechvermögen des PIN Dioden Strahlverlustmonitors, Internal Note: PKTRnote No. 91 (1993).
[53] E. Morré, *Eine Untersuchung für das Zeus-Experiment*, Diploma thesis, Univ. Hamburg (1992), August 1992, 70 p.
[54] H. Burkhardt and I. Reichel, Correction of the LEP beam loss monitors for known saturation effects, CERN SL Note 96–26 OP.
[55] S. Schlögl, *Einsatz von PIN-Photodioden als Protonen-Strahlverlustmonitore bei HERA*, Diploma thesis, DESY-HERA 92–03.
[56] K. Wittenburg, Reduction of the sensitivity of pin diode beam loss monitors to synchrotron radiation by use of a copper inlay, DESY HERA 96–06.
[57] F. Ridoutt, *PIN-Strahlverlustmonitore und ihre Anwendung in dem HERA-Electronen-Ring* (in German), Diploma thesis, DESY-HERA-95–08.
[58] K. Wittenburg, Improvements of the HERA electron beam loss monitor system, Internal Note DESY MDI-99-02.

[59] Bergoz Instrumentation, http://www.bergoz.com/products/BLM/BLM.html.
[60] V. Agoritsas and C. Johnson, EMI aluminum cathode electron multipliers: CERN tests, CERN MPS/CO Note 71–51 (1971).
[61] L. Fröhlich, Experience from the commissioning of the FLASH machine protection system, *Proc. 37th ICFA Advanced Beam Dynamics Workshop on Future Light Sources*, Hamburg, Germany, 2006.
[62] L. Fröhlich, First operation of the flash machine protection system with long bunch trains, *2006 Linear Accelerator Conference*, Linac06, Knoxville, TN.
[63] Nuclear radiation detector type 9841 (aluminum cathode electron multiplier), Thorn EMI, Technical Data sheet (1989).
[64] Saint-Gobain: http://www.detectors.saint-gobain.com.
[65] Electron Tubes, Technical papers, http://www.electron-ubes.co.uk/info/papers.html and Hamamatsu Handbook
` http://sales.hamamatsu.com/assets/pdf/catsandguides/PMT_handbook_v3aE.pdf.
[66] J.R. Parker *et al*., A beam-spill monitor for LAMPF, *IEEE Trans. Nucl. Sci*. **18** (1971) 825–826.
[67] J. Cohen-Tanugi *et al*., Optical properties of the DIRC fused silica Čerenkov radiator, SLAC PUB-9038.
[68] A. Pietryla, W. Berg and R. Merl, A Cherenkov radiation detection system for the advanced photon source storage ring, *Proc. 2001 Particle Accelerator Conference,* Chicago, IL, 2001.
[69] J. Perry *et al*., The CEBAF beam loss sensors, *Proc. 15th IEEE Particle Accelerator Conference*, Washington, D.C., 1993.
[70] E. Janata and M. Körfer, Radiation detection by Čerenkov emission in optical fibers at TTF, Tesla-Report 2000-27.
[71] T. Kawakubo *et al*., High speed beam loss monitor and its deterioration by radiation, *Proc. 9th European Particle Accelerator Conference*, EPAC'04, Lucerne, Switzerland, 2004.
[72] P. Gorodetzky *et al*., Quartz fiber calorimetry, *Nucl. Instrum. Methods Phys. Res*. **A361** (1995) 161–179.
[73] M. Korfer *et al*., Beam loss position monitor using Čerenkov radiation in optical fibers, *Proc. 7th European Workshop on Beam Diagnostics and Instrumentation for Particle Accelerators*, Lyon, France, 2005.
[74] F. Rüdiger *et al*., Beam loss position monitoring with optical fibres at DELTA, *Proc. 11th European Particle Accelerator Conference*, EPAC'08, Genoa, Italy, 2008.
[75] H. Henschel *et al*., Optical fiber dosimeter for SASE FEL undulators, *Proc. 6th European Workshop on Diagnostics and Beam Instrumentation,* DIPAC03, Mainz, Germany, 2003.